1994-03

A constant-depth scratch test for the measurement of adhesion at film-substrate interfaces

Secor, E. Daniel.

Monterey, California. Naval Postgraduate School

NAVAL POSTGRADUATE SCHOOL
MONTEREY, CALIFORNIA

THESIS

A CONSTANT-DEPTH SCRATCH TEST FOR THE MEASUREMENT OF ADHESION AT FILM-SUBSTRATE INTERFACES

by

E. Daniel Secor

March 1994

Thesis Advisor: Indranath Dutta

Unclassified

Security Classification of this page

REPORTS DOCUMENTATION PAGE

1a Report Security Classification: Unclassified	1b Restrictive Markings
2a Security Classification Authority	3 Distribution Availability of Report: Approved for public release; distribution is unlimited.
2b Declassification/Downgrading Schedule	5 Monitoring Organization Report Number(s)
6a Name of Performing Organization: Naval Postgraduate School; 6b Office Symbol (*If Applicable*): 34	7a Name of Monitoring Organization: Naval Postgraduate School
6c Address (*city, state, and ZIP code*): Monterey , CA 93943-5000	7b Address (*city, state, and ZIP code*): Monterey, CA 93943-5000
8a Name of Funding/ Sponsoring Organization; 8b Office Symbol (*If Applicable*)	9 Procurement Instrument Identification Number
8c Address (*city, state, and ZIP code*)	10 Source of Funding Numbers
Program Element Number; Project No.	Task; Work Unit Accession No.

11 Title (Include Security Classification)
A CONSTANT-DEPTH SCRATCH TEST FOR THE MEASUREMENT OF ADHESION AT FILM-SUBSTRATE INTERFACES

12 Personal Author(s)
E. Daniel Secor

13a Type of Report	13b Time Covered	14 Date of Report (year, month, day)	15 Page count
Master of Science Thesis	From To	March 1994	93

16 Supplementary Notation
The views expressed in this thesis are those of the author and do not reflect the official policy or position of the Department of Defence or the U. S. Government.

17 Cosati Codes:	Field	Group	Subgroup

18 Subject Terms (*continue on reverse if necessary and identity by block number*)
Scratch Test, Interfacial Shear Strength, Thin Films

19 Abstract (*continue on reverse if necessary and identity by block number*)
This thesis reviews the development of the constant-depth Scratch Test for determining the adhesive shear strength of thin film-substrate interfaces, and proposes refinements to the theoretical analyses and experimental approach which were developed earlier. Modifications were made to incorporate a change in indenter orientation (for a Vicker's pyramidal indenter) as a measure to minimize damage during scratching. Additionally, the model was expanded to include the use of a conical indenter. A review of film failure modes was conducted, and the damage mechanism of forward lateral flaking was incorporated into the model. The data acquisition program was changed to reflect these modifications. Improvements were added to the previously constructed apparatus. Preliminary tests were conducted on chromium-on-glass samples, the results of which are also presented.

20 Distribution/Availability of Abstract	21 Abstract Security Classification	
X unclassified/unlimited same as report DTIC users	Unclassified	
22a Name of Responsible Individual: Professor Indranath Dutta	22b Telephone (*Include Area Code*): (408) 656-2851	22c Office Symbol: ME-Du

DD FROM 1473, 84 MAR 83 APR edition may be used until exhausted security classification of this page
All other editions are obsolete Unclassified

Approved for public release; distribution is unlimited.

A CONSTANT-DEPTH SCRATCH TEST FOR THE MEASUREMENT OF ADHESION AT FILM-SUBSTRATE INTERFACES

by

E. Daniel Secor
Lieutenant Commander, United States Navy
B.S.M.E., United States Naval Academy, 1980

Submitted in partial fulfillment of
requirements for the degree of

MASTER OF SCIENCE IN MECHANICAL ENGINEERING

from the

NAVAL POSTGRADUATE SCHOOL
March 1994

Author: [redacted]
E. Daniel Secor

Approved by: [redacted]
Indranath Dutta, Thesis Advisor

[redacted]
Matthew D. Kelleher, Chairman,
Department of Mechanical Engineering

ABSTRACT

This thesis reviews the development of the constant-depth Scratch Test for determining the adhesive shear strength of thin film-substrate interfaces, and proposes refinements to the theoretical analyses and experimental approach which were developed earlier. Modifications were made to incorporate a change in indenter orientation (for a Vicker's pyramidal indenter) as a measure to minimize damage during scratching. Additionally, the model was expanded to include the use of a conical indenter. A review of film failure modes was conducted, and the damage mechanism of forward lateral flaking was incorporated into the model. The data acquisition program was changed to reflect these modifications. Improvements were added to the previously constructed apparatus. Preliminary tests were conducted on chromium-on-glass samples, the results of which are also presented.

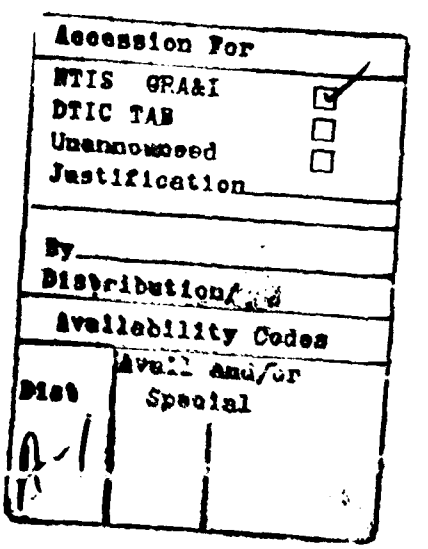

TABLE OF CONTENTS

I. INTRODUCTION

There is a continuing strong interest in the area of thin films on substrates due to the wide applicability in many areas of technology, most notably in the fields of electronics and optics. In the broadest sense, a film of either a polymer or metal is deposited on a substrate of either metal, semi-conductor or ceramic. The purpose of the film may be to modify the properties of the substrate, such as chemical, mechanical, electromagnetic or aesthetic [Ref. 1]. Films are also used to protect the substrate surface from damage due to contact loading, impact or abrasion [Refs. 2, 3]. In the area of electronics packaging, thin films are applied on ceramic substrates to enhance their thermal conductivity or to provide electrical interconnections between devices.

The performance of the film-substrate system is directly related to the properties of the materials used and the strength of the interfacial bond. The larger the mismatch between material properties, the more the interfacial bond is degraded. The interface between dissimilar materials is often the limiting factor of many systems, often yielding inadequate adhesion and/or large residual stresses in the film. With a change in temperature, for example, large strains can be induced in the film, with the resultant interfacial shear stress being sufficient to cause failure of the bond at the interface. Strong adhesion between films and substrates, therefore, is critical.

To this end, a method is desired to determine quantitatively the strength of the interfacial bond; i.e., the interfacial shear strength. Valli [Ref. 4] describes the requirements of such a test as being easy, quick to carry out, and practicable for tools and machine parts. The results should be easy to interpret, and must be recordable electronically for automation purposes.

A. INTERFACIAL ADHESION TESTS

Several methods have been developed to evaluate the adhesion of coatings to substrates. However, each has its limitations and disadvantages. With the improvement of chemical and physical deposition methods, coatings with high adhesion strengths are achievable, and the number of applicable adhesion tests is limited. [Ref. 4]

The pull-off method is a basic test with several techniques by which it is accomplished. One technique involves the use of an adhesive tape or a collodion [Ref. 5 The collodion is allowed to dry over the metal film, and then an attempt is made to strip both films off together. The use of a pressure-sensitive adhesive tape is similar. The tape is applied to the film and then pulled off. Detachment of the film from the substrate implies failure of the interfacial bond. This is a qualitative method, and is good only if the interfacial bond is already known to be weak since the connection between the coating and tape can be limiting. A second technique [Ref. 4] places the film-substrate sample between the ends of two rods. The end of one rod is cemented to the coating while the end of the other rod is cemented to the bottom side of the substrate. The application of a purely normal force will result in detachment of the film from the substrate. A derivative of this technique is the "topple" method [Refs. 4, 6]. Only the end of one rod is cemented to the film. By applying a force to the opposite end of the rod in a direction parallel to the film, the normal stress between the rod and the film is tensile on one edge of the rod, and changes to compressive across the contact area. Again, the adhesive strength of the cement (for example, epoxy) can be a limiting factor. For both techniques mentioned, the effects on the film-substrate interface of the adhesive/cement solvent penetrating the film are not considered. A third form of the pull-off method involves the use of an electromagnetic force [Ref. 4]. A current that is passed through the film reacts with an external magnetic field to produce an outward normal force on the film. This method requires the film to be an electrically conductive material, while the substrate is an insulator.

Another method, though also disadvantaged by the use of adhesive, is the lap shear test. A flat glass plate is cemented to the top surface of the film. The resultant lap joint is pulled to produce a shear stress. While this may test the film-substrate interfacial bond in shear, there is a large scatter in results, which, overall, are lower than expected. Stress distribution in a lap joint is known to be complicated, and stress concentrations depend on many factors. [Refs. 6, 7]

A body-force test can be accomplished in two ways. A coated rotor is suspended in a magnetic field and rotated at increasing velocities until detachment of the coating occurs. Likewise, a small sample can be placed in an ultrasonic cleaning bath, which will then generate body forces similar to that accomplished in the centrifuge. However, in both these methods, the normal force generated is proportional to the mass of the coating. Experimentation has shown that a relatively thick coating (250μ) is required to result in a force causing detachment. Since, in many practical applications, the thinnest film is desired, these methods would not be appropriate. Additionally, these methods are not applicable to tools or components. [Refs. 4, 6]

In the heat and quench test, the film-substrate sample is heated to a predetermined temperature based on the material properties of the sample. Subsequent quenching results in thermal stresses being generated; the thermal shock may or may not cause film detachment. Reactions of the materials to high temperatures, such as oxidation, are not considered in this qualitative-only method. [Ref. 4]

Nucleation methods are based on the observation of the kinetics of thin film formation. On the microscopic level, removing an atom of film consists of breaking the bonds between adjacent atoms and the substrate. Therefore, on the macroscopic level, removing the film can be considered as a summation of the individual atomic forces. Nucleation methods relate the absorption energy of the single atom on the substrate to the total adhesion of the film. The absorption energy determines the time required for an atom to condense on the

substrate during film deposition. Hence, observations of the film build-up with an electron microscope can give measurements from which the absorption energy can be derived [Ref. 8]. However, this method cannot be used to test the adhesion of thin films on practical tools or machine parts [Ref. 4].

A fairly recent method employs a laser in a technique called "laser spallation." A high-energy laser beam is directed towards the bottom side of the substrate. The resultant compressive shock waves are transmitted through the substrate to the film-substrate interface. The power of the laser is raised until the shock waves are of sufficient intensity to cause detachment. As expected, this method can be quite complex and expensive relative to more conventional methods. Also, it measures the normal interfacial strength, and not the shear strength. Another limitation of this method is that the film must be deposited in a pattern of dots that are smaller in diameter than the width of the laser beam. [Ref. 4]

In an indentation test [Refs. 9, 10], the indenter (usually a ball or Vicker's indenter) is loaded against the coated surface of the sample piece. The coating is displaced laterally as the load on the indenter is increased. The lateral motion causes a shear stress to develop across the film-substrate interface. Debonding occurs at a sufficiently high indenter load, and this in turn, is related to the interfacial shear strength. However the instant of interfacial failure can be difficult to detect. If the substrate is transparent, the test process can be viewed with a microscope from beneath the sample. *In situ* monitoring then permits one to observe the moment of failure. If the substrate is not transparent, the use of acoustic monitoring can reveal failure; however, the emissions of failure may be indistinguishable from or masked by the emissions due to cracking in the film and/or substrate. Because of its application to this thesis, the mechanics of this test will be discussed in more detail later.

Another test that estimates the interfacial shear strength is the scratch test. In this method, the indenter is pulled across the coated surface as the normal force is increased continuously or in a step-wise fashion [Refs. 4, 11, 12]. At some critical load P_c, damage

transpires in the vicinity of the scratch, and detachment of the film occurs. The load at detachment gives a comparable value of the film adhesion, though this is strongly dependent on many variables, such as film thickness or roughness. The details of the scratch test, and the relevance of the indentation test to the scratch test, will now be discussed.

B. REVIEW OF THE INDENTATION AND SCRATCH TESTS

1. Indentation Test

By applying a vertical load with either a spherical or Vicker's indenter onto the film, the resultant compressive stresses cause a lateral displacement of the film with respect to the substrate. This develops a shear stress across the film-substrate interface. Matthewson [Ref. 3] initially studied the stresses of thin soft films by the use of indentation. He developed analytical models for determining the stresses within the coating for various indenter profiles. He later [Ref. 1] used these models to formulate equations to determine the shear strength at the film-substrate interface. As the indenter load is increased to some critical load P_c, failure of the interfacial bond occurs. Ritter et al. [Refs. 2, 7, 9] identified three types of failure of the interface. These are shown in Figure 1.1. In Type I, the indenter causes elastic deformation of the film to the point of debonding. Debonding occurs before the film is penetrated. Type II failure occurs when the film is plastically deformed prior to debonding, again before penetration of the film. In Type III failure, as in Type II, there is plastic deformation of the film, but it is completely penetrated prior to failure. It was expected that spherical indenters would cause Types I or II debonding, whereas a sharp indenter would cause Types II or III debonding. Since the substrate used by Ritter was transparent, this process was observed directly. For translucent or opaque materials, though, the instant of debonding is difficult to determine,

and is usually detected using ultrasonic or acoustic systems. Types II and III failures will be discussed later in the theoretical modeling.

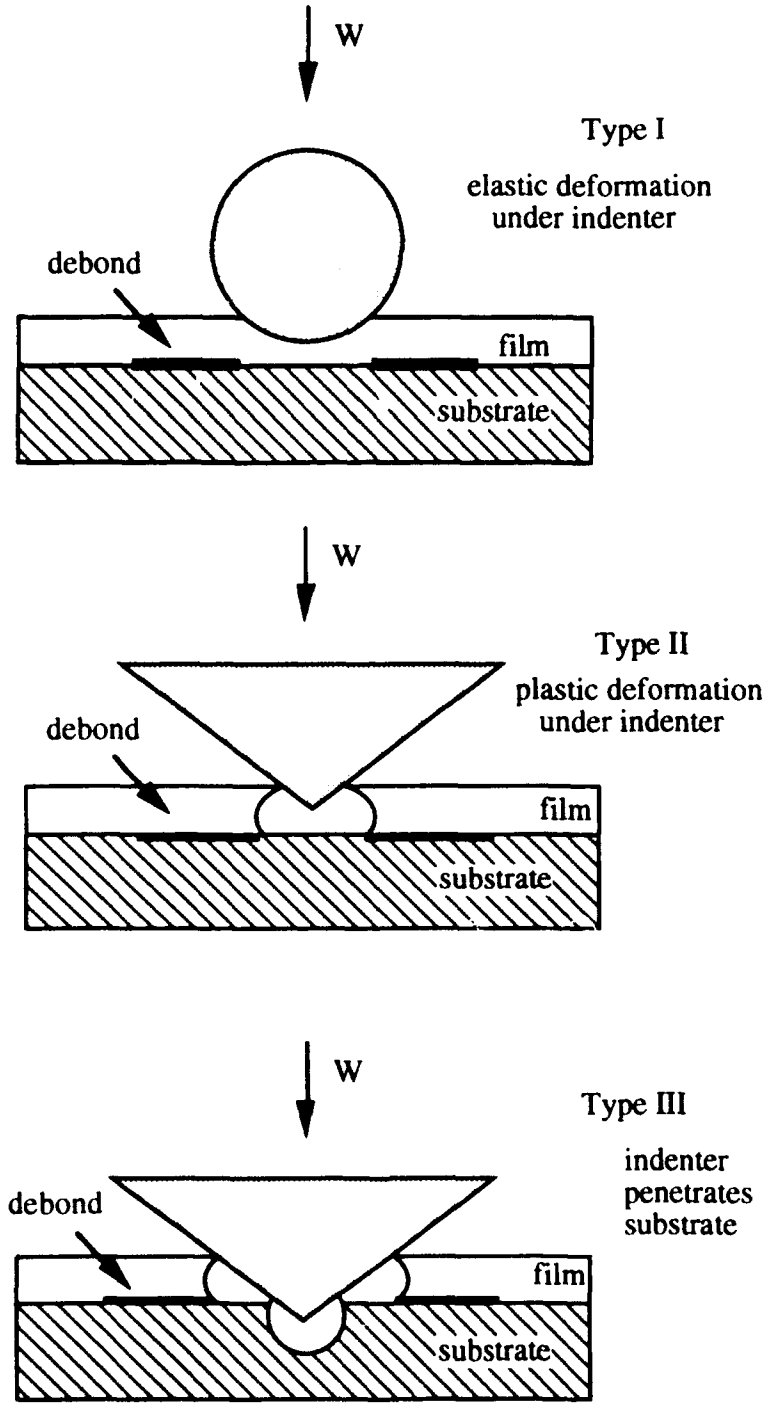

Figure 1.1: Three Types of Failure [Ref. 9].

2. Scratch Test

The scratch test was first used by O.S. Heavens in the early 1950's to determine the adhesion of chromium films on glass. He used a steel ball indenter pulled across the sample with a continuously increasing normal force applied to the indenter. The critical value was defined as the point when the film was stripped away from the substrate, leaving a clean channel. The normal load at this point was simply a comparative value - a measure of the adhesion of the film [Ref.13]; the value did not correspond to any particular material or film-substrate system property. Benjamin and Weaver used the same method to attach a quantitative number to the results of the test. They formulated an equation relating the shear stress due to surface deformation and the critical load. The results were of the same order of magnitude as the results of nucleation methods, but works by Butler et al. indicated that the film failure was more complicated than Benjamin and Weaver had predicted. For example, the instant of film failure proved to incur large errors. Where Heavens defined failure as a "clean channel," Butler et al. indicated that the detached film could remain in the vicinity of its original location without breakage; or, the film could be thinned by the indenter to translucence such that it appeared to have been detached, although it was still intact [Ref. 14].

Several works were conducted involving the monitoring of the scratch test, and specifically, the moment of interfacial failure. Butler et al. [Ref. 14] observed the scratches after the test using electron and optical microscopy. An attempt was made to note adhesion failure with strain gauges monitoring the frictional force, but an indicative change in force was not detectable, possibly due to, as Lascurain [Ref. 15] noted, reduced sensitivity of available strain gauges. Several years later in the 1970's, Maan and Van Groenou [Ref. 16] monitored the scratch process using a TV camera and a bending element with strain gauges. Even though the primary purpose of their research was the evaluation of the effects of indenter velocity, Maan and Van Groenou were able to obtain accurate frictional

force data. Valli et al. [Refs. 11, 17] used both acoustic emission and frictional force measurements to note when film failure occurred. While both measurements provided indication of film failure at film thicknesses above 1.5μ, acoustic emissions provided questionable information at a film thickness of 0.8μ, below which no indicative acoustic emission was provided. Sekler et al. [Ref. 18] conducted research comparing the use of acoustic emission, microscopy, and force measurements to determine film failure. The force measurements provided limited information, and were most useful when performed in combination with acoustic emission and/or microscopy results. For films of thicknesses less than 0.5μ, scratch testing could not be used to characterize adhesion properties, except in rare cases. This limitation was due to the inability of a scratch tester to apply a force of magnitude 0.01 newtons or less. In fact, Sekler et al. concluded that the development of a scratch tester with such an ability would enable the characterization of films with drastically reduced thicknesses.

Several factors affecting the results of the scratch test can cause deviations of about 10-20% of the reading [Ref. 4]. These factors include the substrate hardness, coating hardness, surface roughness, and loading rate. The effects of these are discussed at length by Valli [Refs. 4, 11, 17], Butler [Ref. 14], and Lascurain [Ref. 15]. Other factors affecting the results and conduct of the scratch test specifically addressed in this thesis are indenter orientation, friction between the indenter and film, and coating thickness.

Maan and Van Groenou [Ref. 16] conducted low-speed scratch experiments on steel using a Vicker's indenter. They conducted the scratch testing with the indenter oriented with a leading plane. This reduced the complexities associated with the shear stress resolution along the contact planes. Material flow along a contact plane implies a shear stress exists. With a leading edge orientation, the contact planes are not parallel to the direction of motion (Figure 1.2). While some studies are based on the assumption that any

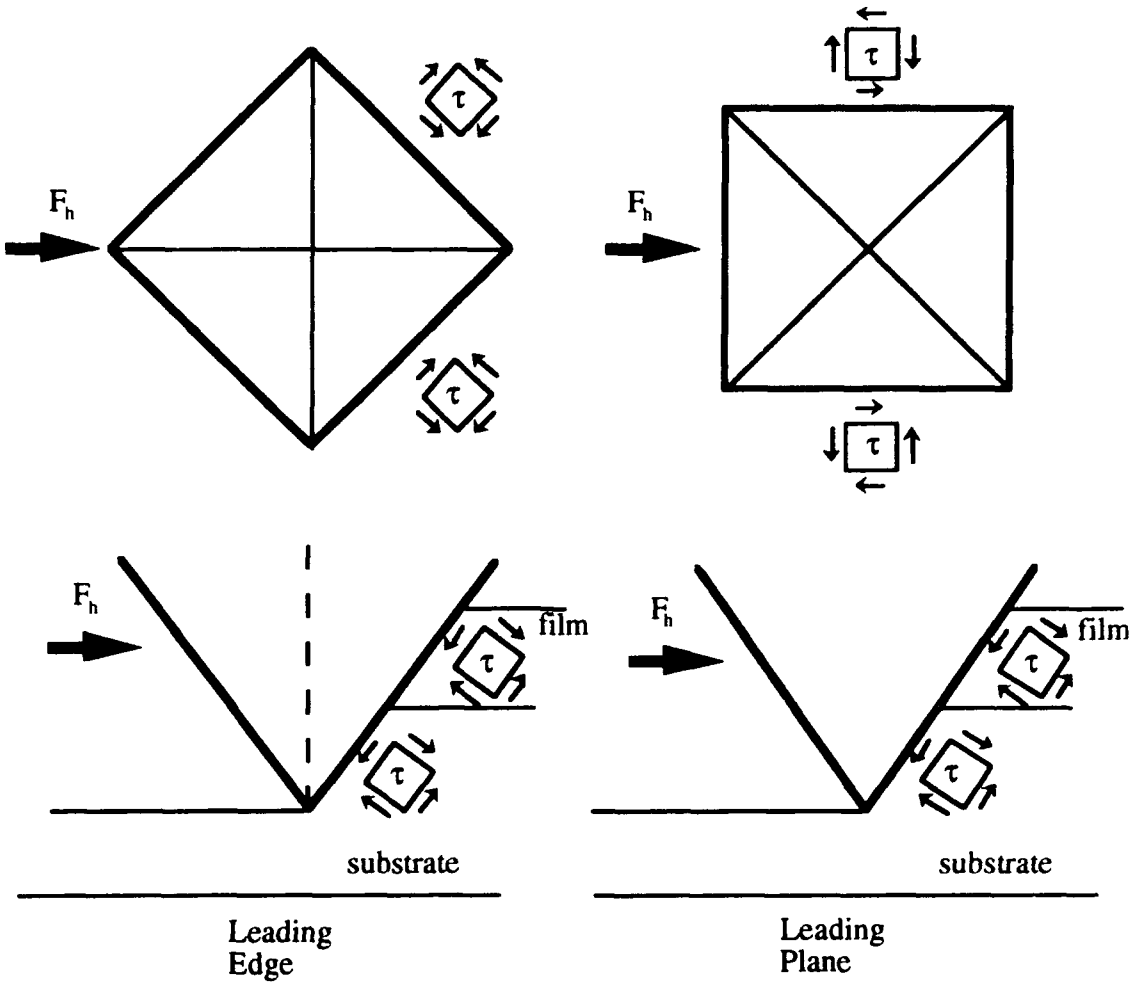

Figure 1.2: Orientation of Shear Stresses with Respect to Indenter Motion. shear stresses are parallel to the surface in the direction of scratch velocity, others assume the shear is parallel to the projection of the velocity on the contact planes. Additionally, there is little knowledge of the three-dimensional stresses and strains beneath the inclined contact planes, regardless of the indenter orientation. Maan and Van Groenou assumed that with a leading plane, compression only would occur on that plane, and any flow around the sharp corners would be unlikely. With this orientation, the two planes over which any shear stresses act are now parallel to the direction of motion. While this may not be the

answer to the three-dimensional stress/strain question, it did resolve the stresses in the horizontal plane.

Little research has been done on the use of lubricants for the scratch test. Valli et al. [Refs. 4, 11, 17] conducted scratch tests using four different coating-lubricant combinations: TiN as coated, TiN & silver, TiN & oil, and TiN & silver & oil. They concluded that friction can be a dominant factor affecting the results. The application of a solid lubricant, such as silver, did raise the critical normal force. While pure oil did not affect the critical load causing interfacial debonding, it did enhance the repeatability of the testing (Figure 1.3). The relative humidity of ambient air caused scatter in the results, especially with tests involving optical coatings on glass [Ref. 4]. Considering the care necessary to ensure cleanliness between the indenter and the coating, the application of a lubricant may have served to seal out airborne contaminants or moisture.

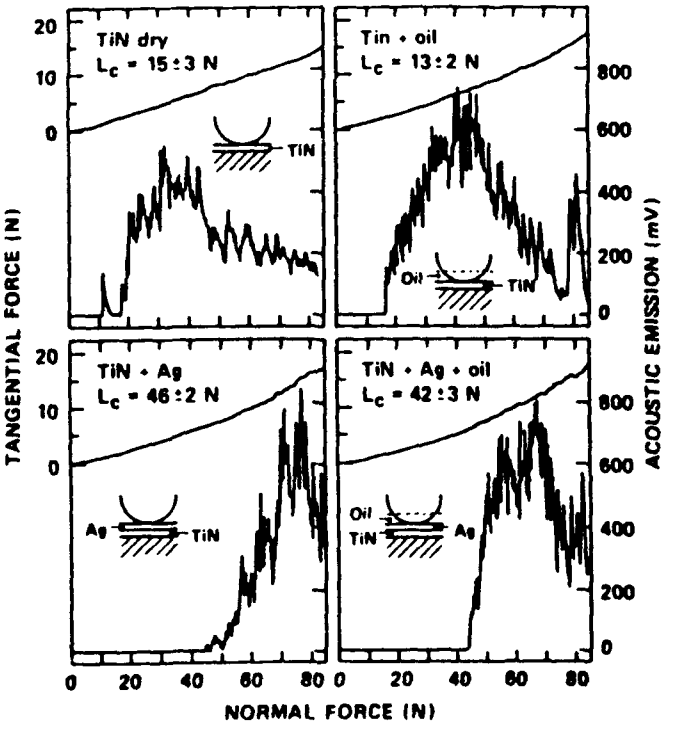

Figure 1.3: Effects of Lubrication on Scratch Testing [Ref. 3].

As a rule, the critical normal force P_c increases as the film thickness increases [Refs. 4, 6, 19] (Figure 1.4). In some situations, P_c will reach a maximum value based on the material properties of the substrate. This may be due to substrate deformation. Additionally, as the thickness increases, there is the propensity for internal stresses to exist as a result of the film deposition process. The effect of this may actually reduce the ability of the film-substrate to withstand a normal force without interfacial failure.

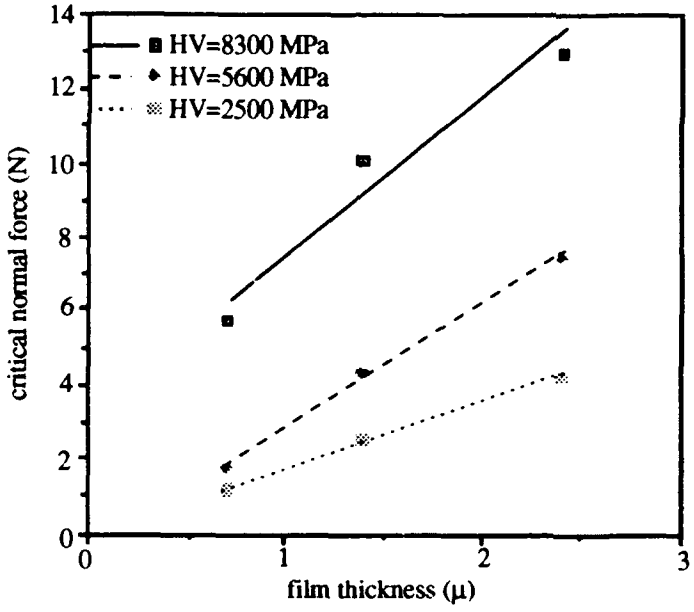

Figure 1.4: Critical Normal Force vs. Film Thickness [Ref. 12].

As discussed earlier, one of the sources of error in a scratch test reading is the definition of interfacial failure. Hedenqvist et al. [Ref. 19] and Bull [Ref. 20] have recently studied the modes of failure and their relevance to scratch testing. Although only a few of the modes observed and defined by Bull are related to the film-substrate interface failure, other modes may result in a particular behavior of the material in another application. Hence, the study of those modes, though unrelated to the scratch test, is important. Bull categorized his efforts based on whether the substrate behaved in a brittle or ductile manner. His observations resulted in the classification of several modes of failure each for brittle and ductile substrates (Figure 1.5). Hedenqvist et al. used a scratch test apparatus in

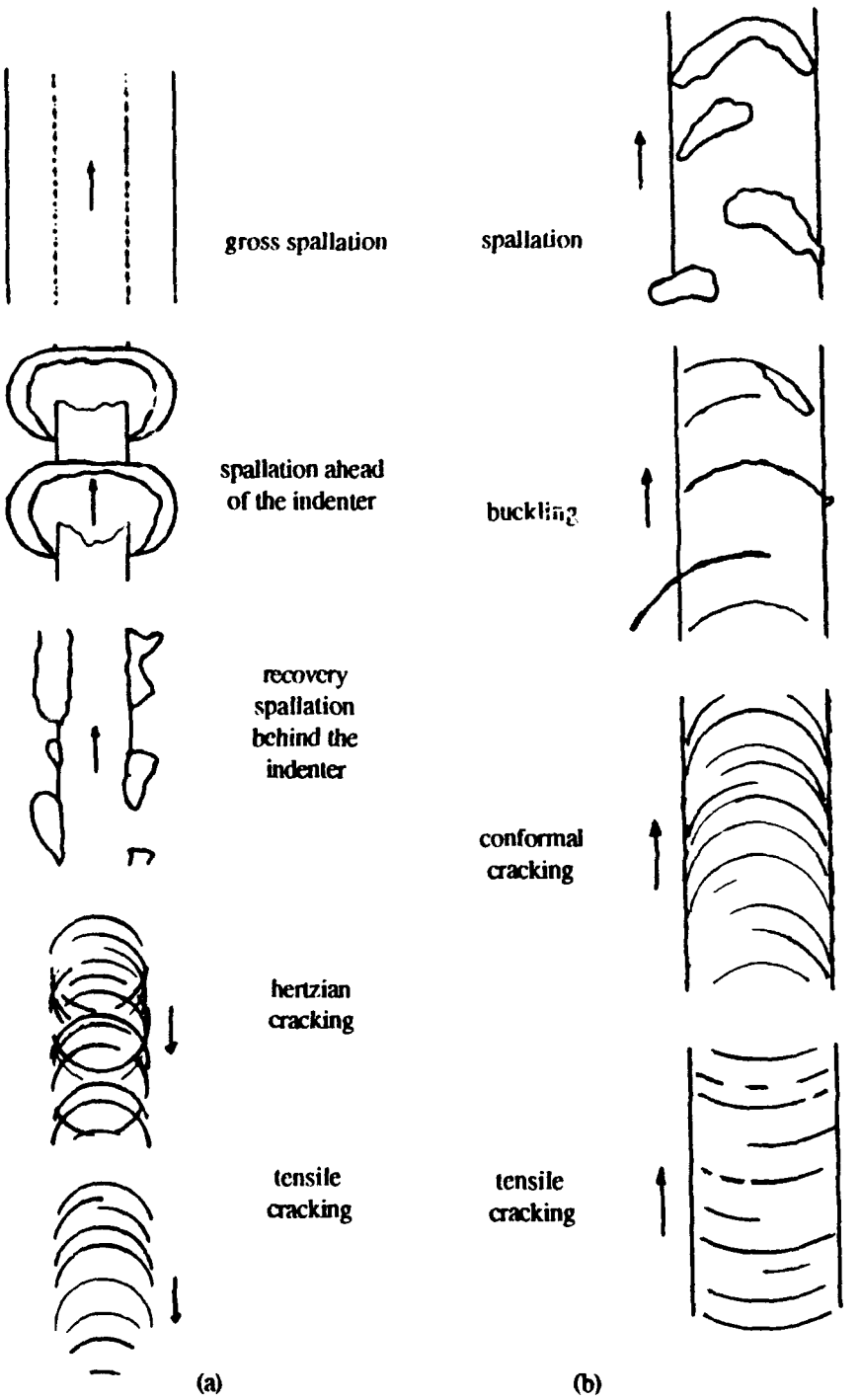

Figure 1.5: Failure Modes in Scratch Testing: (a) Brittle Substrate; (b) Ductile Substrate [Ref. 20].

conjunction with a scanning electron microscope. This permitted *in situ* testing of film adhesion, thereby allowing the researchers to observe the dynamics of the film failure. Failures were categorized by the damage and detachment process involved (Figure 1.6). *In situ* monitoring proved to be significant in that the results of different modes of failure appeared similar, but the actual process of failure was quite different.

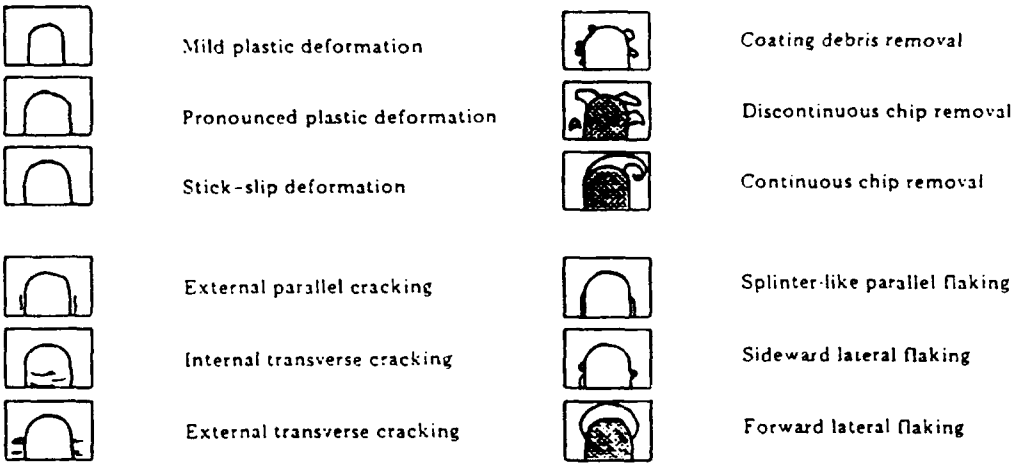

Figure 1.6: Mechanisms of Coating Damage and Detachment [Ref. 19].

Since a glass substrate is used for the samples tested as part of this thesis, Bull's observations for brittle substrates are applicable. A common failure mode for this category is a form of spallation. The amount of spallation is a function of the interfacial adhesion and any residual stresses in the coating. For a weak interface and high residual stresses, a crack in the coating is formed at the point of contact with the indenter. This crack propagates a considerable distance on either side of the scratch track, resulting in large flakes of the film falling away from the track area (gross spallation, Figure 1.5(a)). When the residual stresses are low (or non-existent) and the adhesion is better than that described above, spallation still occurs, but to a lesser degree. The motion of the indenter produces compressive stresses in front of the indenter. As a mechanism of relieving these stresses and reducing the stored elastic energy, semicircular cracks will form and propagate

outwards from the track center. If the crack is through the film, chips will be removed from the track (spallation ahead of the indenter, Figure 1.5(a)). This mode of failure becomes more probable as the film thickness increases [Ref. 20]. Hedenqvist et al. identified a similar damage mechanism as forward lateral flaking. Again, compressive stresses build up in front of the moving indenter, but rather than forming cracks as Bull concluded, Hedenqvist observed that the coating buckles, resulting in the removal of semicircular flakes. This mechanism is associated with interfacial spalling [Ref. 19]. The identification of any possible modes of failure becomes a significant part of the modeling of the scratch test. Whether using acoustic emissions or force measurements to determine interfacial failure, that measurable quantity may be influenced by the energy associated with the initiation and continuation of the damage mechanism. Not accounting for that influence can cause errors in the experimental results.

In his graduate work [Ref. 15], Lascurain developed a simple, straightforward test adaptable to the testing of the adhesion of thin films to ceramic substrates. Load cells were used to monitor the normal and tangential forces during the scratch process. Since complete removal of the film during the scratching process would be assured if the indenter had penetrated into the substrate, a predetermined load (just less than that required for Type III indentation debonding) was applied to the indenter prior to scratching. Rather than controlling the normal force during the scratch process, the depth of the indenter was maintained constant. This reduced the complexities and possible errors of the test, such as junction growth due to the changing geometry as the indenter depth varied. The resultant normal force and the tangential force to produce the relative motion between the indenter and film were monitored. Lascurain developed an analytical expression relating these forces to the interfacial shear strength. This approach eliminated the need for determining the precise moment at which the film debonded from the substrate, thus simplifying the experimental method considerably.

C. OBJECTIVES

The purpose of this thesis is to continue the research started by Lascurain. The results of works by Maan et al. [Ref. 16], Hedenqvist [Ref. 19], and Bull [Ref. 20] will be incorporated into the modified analytic expressions. Improvements will be made to the scratch tester apparatus and its modifications designed by Lascurain to overcome some physical limitations. An expression for the use of a conical indenter will be introduced. Finally, tests will be conducted on chromium-on-glass samples, and some sample results will be presented.

II. THEORETICAL MODELING

A. REVIEW OF INDENTATION DEBONDING (VICKER'S INDENTER)

In developing a model for Type II failure in which the film is plastically deformed prior to debonding, Ritter et al. used the results of earlier studies [Refs. 1, 3] conducted by Matthewson. Matthewson had modeled the compressive stresses in the film beneath a spherical indenter (Figure 2.1) as a cylindrical cavity under an internal pressure as shown in Figure 2.2. From this, Ritter et al. derived an expression for the shear stress at the film-substrate interface:

$$\tau = \frac{\sigma_r}{\frac{k_1'(z)}{k_1(z)\phi} + \frac{\nu\, t}{a\phi^2}} \qquad (2.1)$$

where σ_r is the radial stress generated in the film by the indenter, a is the radius of the film-indenter contact area, ν is the Poisson's ratio of the film, t is the film thickness, $k_1(z)$ is a

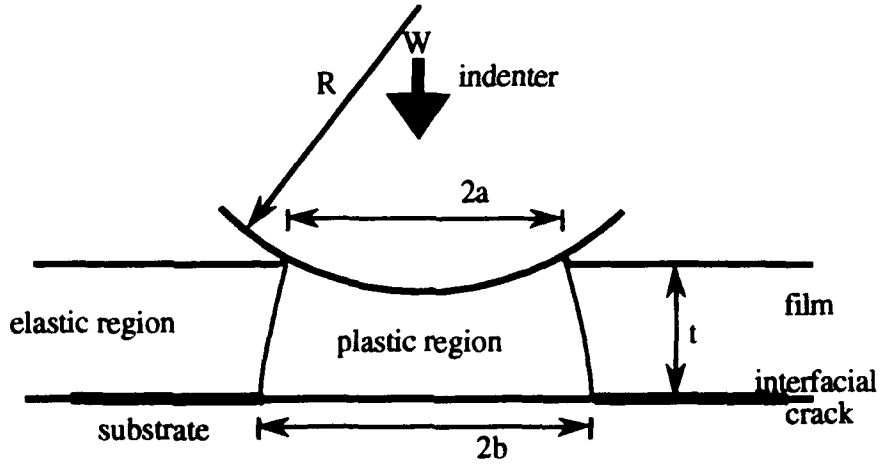

Figure 2.1: Schematic of Indentation Experiment Showing Interfacial Crack [Ref. 1].

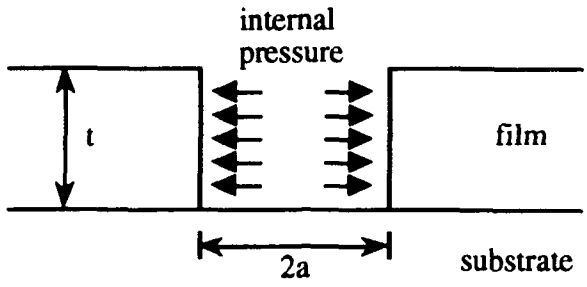

Figure 2.2: Model System for Indentation [Ref. 1].

modified Bessel function of the second kind to the first order, and $k_1'(z)$ is its derivative with respect to z. ϕ is a constant, given by:

$$\phi = \sqrt{\frac{6(1-\nu)}{(4+\nu)}} \qquad \text{and} \quad z = \frac{a\phi}{t} \tag{2.2}$$

The expansion of the modified Bessel function and its derivative are shown in Appendix F. Equation 2.1 is also applicable to a Vicker's pyramidal indenter [Ref. 2], where a is replaced by b, the half diagonal length of the film-indenter contact area (Figure 2.3). σ_r in equation 2.1 is related to the film indentation hardness H_f by the equation (see Appendix A):

$$\sigma_r = -0.6875\, H_f \quad \text{where} \quad H_f = \frac{W}{2b^2} \tag{2.3}$$

and W is the indentation load. Substituting for σ_r in equation 2.1, the following is obtained:

$$\tau_{iv}^{II} = \frac{-0.6875\left[\frac{W}{2b^2}\right]}{\frac{k_1'(z)}{k_1(z)\phi} + \frac{\nu\, t}{b\phi^2}} \tag{2.4}$$

Here, τ_{iv}^{II} is the Type II interfacial shear stress due to the vertical load. When W represents the critical load required to just initiate interfacial failure, τ_{iv}^{II} represents the shear strength of the interface.

When considering Type III debonding, the load W is now supported by both the film and the substrate (Figure 2.4) [Ref 2]. Since W is distributed over the projected areas of the film and substrate, A_f and A_s (Figure 2.3), respectively,

$$\begin{aligned} W &= A_f H_f + A_s H_s \\ &= 2(b^2 - c^2)H_f + 2(c^2)H_s \end{aligned} \tag{2.5}$$

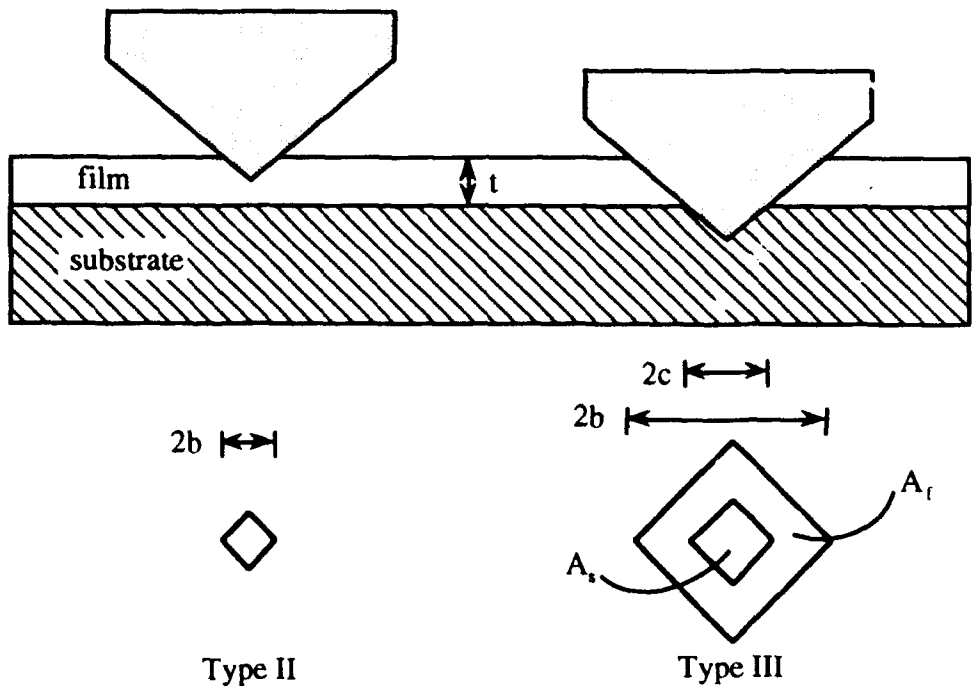

Figure 2.3: Geometry of Types II and III Debonding for Pyramidal Indenter [Ref. 15].

Solving for the film indentation hardness H_f yields:

$$H_f = \frac{W - 2c^2 H_s}{2(b^2 - c^2)} \tag{2.6}$$

Of note is the ease of which H_f can be obtained. W is continuously measured during the scratch test, b is measured using the Vicker's micro hardness tester measuring eyepiece, and c can be calculated based on the known geometry of the Vicker's pyramidal indenter. Using the relationship of equation 2.6 for H_f, equation 2.4 becomes [Ref. 2]:

$$\tau_{iv}^{III} = \frac{-0.6875\left[\frac{W - 2c^2H_s}{2(b^2 - c^2)}\right]}{\frac{k_1'(z)}{k_1(z)\phi} + \frac{\nu\, t}{b\phi^2}} \qquad (2.7)$$

Here τ_{iv}^{III} represents the interfacial shear stress due to the indentation when debonding is of Type III classification.

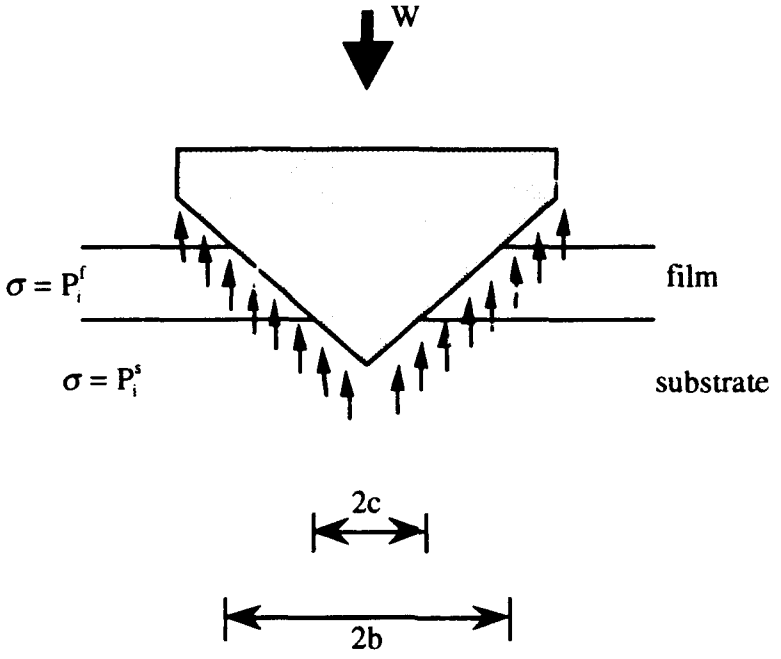

Figure 2.4: Schematic of Load Sharing for Type III Debonding (from Howes and Ryan Model [Refs. 2, 15].

B. SCRATCH TEST (VICKER'S INDENTER)

1. Leading Edge Orientation

Up to this point the indenter has been stationary so that its orientation with respect to the proposed scratch track is irrelevant. When the horizontal force is applied, though, the orientation will affect the interfacial shear strength which is generated due to the horizontal force.

As the horizontal force is applied during the scratch test, the indenter is no longer supported by the projected areas, A_f and A_s. This is due to the removal of the film and

substrate materials in the scratch track behind the indenter. This is shown in Figure 2.5. Equation 2.5 becomes:

$$W = \tfrac{1}{2}\left(A_f H_f + A_s H_s\right) = (b^2 - c^2)H_f + c^2 H_s$$

$$\Rightarrow \quad H_f = \frac{W - c^2 H_s}{b^2 - c^2} \tag{2.8}$$

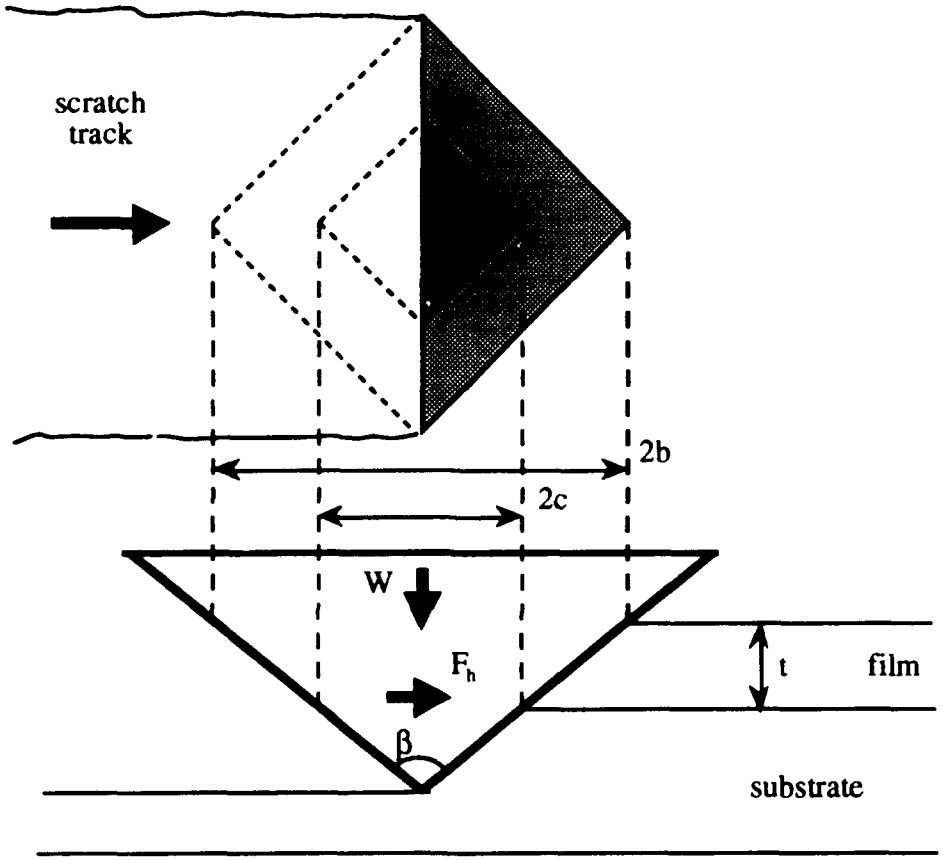

Figure 2.5: Projected Areas of Pyramidal Indenter in Contact with Film and Substrate during Scratching.

Substituting equation 2.8 into equation 2.7 produces:

$$\tau_{ihv}^{III} = \frac{-0.6875\left[\dfrac{W - c^2 H_s}{b^2 - c^2}\right]}{\dfrac{k_1'(z)}{k_1(z)\phi} + \dfrac{\nu\, t}{b\phi^2}} \tag{2.9}$$

where τ_{ihv}^{III} represents the Type III shear stress at the interface due to the vertical load when a horizontal force is applied.

In the scratch test developed by Lascurain, a horizontal force F_h is applied to the translation table on which the test sample is placed. The sample, which is beneath the fixed indenter, then moves relative to the indenter, and causes the scratch to be generated. The force applied must overcome several opposing forces as determined by Benjamin and Weaver [Refs. 13, 21]. These include:

- the force to plough through the film, P_f;
- the force to plough through the substrate, P_s;
- the force to overcome the shear stress between the indenter and the film, $F_{f/ind}$;
- the force to overcome the shear stress between the indenter and the substrate, $F_{s/ind}$; and
- the force to overcome the shear strength of the film-substrate interface, F_{ieff}.

The force to plough through the film is defined [Ref. 15] as:

$$P_f = AH_f = [(b+c)t]\left[\frac{W - c^2 H_s}{b^2 - c^2}\right] \tag{2.10}$$

where A is the projected area over which the force acts.

The P_s term is also based on the indentation hardness and the projected area in front of the indenter [Ref. 15].

$$P_s = H_s c^2 \cot(\beta/2) \tag{2.11}$$

where β is the angle (148.1°) between opposite edges of the Vicker's indenter (Figure 2.5).

The forces to overcome the shear stress between the indenter and film, and between the indenter and substrate, are defined [Ref. 15] as:

$$F_{f/ind} = S_{f/ind}(b^2 - c^2) \tag{2.12}$$

and

$$F_{s/ind} = S_{s/ind} c^2 \tag{2.13}$$

based on works by Benjamin and Weaver [Ref. 13]. $S_{f/ind}$ and $S_{s/ind}$ are the average shear strengths of the film and substrate, respectively. Lascurain combined the Von Mises stress theory together with the works of Bowden and Tabor [Ref. 22] to derive the relationships:

$$S_{f/ind} \approx \frac{H_f}{5.5} = \frac{W - c^2 H_s}{5.5\left(b^2 - c^2\right)} \quad \text{and} \quad S_{s/ind} \approx \frac{H_s}{5.5} \tag{2.14}$$

With these substitutions, equations 2.12 and 2.13 become:

$$F_{f/ind} = \frac{W - c^2 H_s}{5.5} \tag{2.15}$$

and

$$F_{s/ind} = \frac{H_s c^2}{5.5} \tag{2.16}$$

The force to overcome the shear stress at the film-substrate interface F_{ieff} can be defined as:

$$F_{ieff} = \tau_{ieff} c^2 \tag{2.17}$$

However, τ_{ieff} does not represent the shear strength of the interface since part of the shear strength is overcome by the application of the vertical load of the indenter. If τ_i is the interfacial shear strength, then

$$\tau_i = \tau_{ihv}^{III} + \tau_{ieff} \tag{2.18}$$

where all three shear values are acting over the same area c^2, which is the footprint of the indenter on the film-substrate interface. Combining the five components of F_h, the following equation is produced:

$$F_h = P_f + P_s + F_{f/ind} + F_{s/ind} + \tau_{ieff} c^2 \tag{2.19}$$

Solving for τ_{ieff} (using equations 2.10, 2.11, 2.15, and 2.16), substituting τ_{ieff} into equation 2.18, and then using equation 2.9 to substitute for τ_{ihv}^{III} yields [Ref. 15]:

$$\tau_i = \frac{F_h}{c^2} - H_s\left[\tfrac{1}{5.5} + \cot\left(\tfrac{\beta}{2}\right)\right] - \frac{W - c^2 H_s}{b^2 - c^2}\left[\frac{\left(b^2 - c^2\right)}{5.5c^2} + \frac{(b+c)t}{c^2} + \frac{0.6875}{\frac{k_1'(z)}{k_1(z)\phi} + \frac{\nu\, t}{b\phi^2}}\right] \tag{2.20}$$

This is the expression that was obtained for the interfacial shear strength by Lascurain [Ref. 15].

2. Leading Plane Orientation

Maan and Van Groenou [Ref. 16] concluded that a leading plane orientation reduces the complexities associated with the material flow along the contact planes since the flow is parallel to the direction of velocity. A change to this orientation involves geometry changes as follows. Note the relationship between b' and b in Figure 2.6(a). As seen in Figure 2.6(b), when the horizontal force is applied to the indenter, and the scratch is

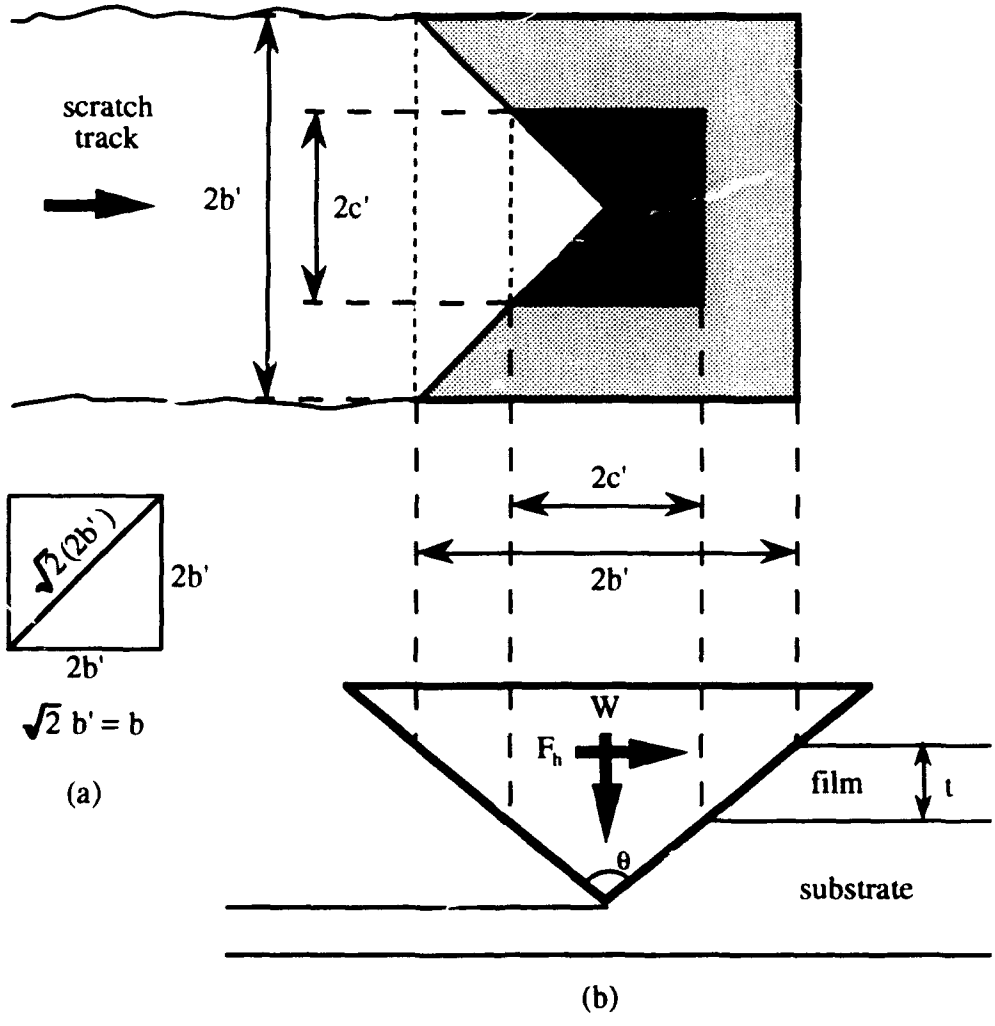

Figure 2.6: Leading Plane Geometry: (a) Relationship between b and b'; (b) Projected Areas of Indentation during Scratching.

generated, the vertical load is supported by only three quarters of the projected area of the indenter. Referring to equation 2.5:

$$W = A_f H_f + A_s H_s = \tfrac{3}{4}\left[(4b'^2 - 4c'^2)H_f + (4c'^2)H_s\right]$$

$$\Rightarrow \quad H_f = \frac{W - 3H_s c'^2}{3(b'^2 - c'^2)} \tag{2.21}$$

Accordingly, the force to plough through the film P_f (from equation 2.10) is rewritten as:

$$P_f = AH_f = [(b' + c')t]\left[\frac{W - 3H_s c'^2}{3(b'^2 - c'^2)}\right] \tag{2.22}$$

where A is the projected area of the leading plane in contact with the film.

The force to plough through the substrate P_s (from equation 2.11) is revised as:

$$P_s = AH_s = c'^2 H_s \cot(\theta/2) \tag{2.23}$$

where A is now the projected area of the leading plane in contact with the substrate (see Appendix B), and θ is the angle (136°) between opposite planes of the Vicker's indenter (Figure 2.6).

To revise the force to overcome the shear stress between the indenter and the film $F_{f/ind}$ (from equation 2.12):

$$F_{f/ind} = S_{f/ind} A = \frac{H_f}{5.5} A_f$$

$$\Rightarrow \quad F_{f/ind} = \frac{2H_f(b'^2 - c'^2)}{5.5 \sin(\theta/2)} \tag{2.24}$$

where A_f is the actual area of contact between the two side planes and the film, and H_f is defined in equation 2.22. Appendix B illustrates the derivation of A_f.

To revise the force to overcome the shear stress between the indenter and the substrate $F_{s/ind}$ (from equation 2.13):

$$F_{s/ind} = S_{s/ind} A = \frac{H_s}{5.5} A_s$$

$$\Rightarrow \quad F_{s/ind} = \frac{2 H_s c'^2}{5.5 \sin(\theta/2)} \tag{2.25}$$

where A_s is the actual area of contact between the two side planes and the substrate (see Appendix B).

To revise the force to overcome the shear stress at the film-substrate interface F_{ieff}:

$$F_{ieff} = \tau_{ieff} A = \tau_{ieff} \left(\tfrac{3}{4} \, 4c'^2 \right) = \tau_{ieff} 3c'^2 \tag{2.26}$$

Combining the components for F_h and solving for τ_{ieff} results in:

$$\tau_{ieff} = \frac{F_h}{3c'^2} - \frac{\tfrac{2}{3} H_s}{5.5 \sin(\theta/2)} - \frac{\tfrac{2}{3} H_f (b'^2 - c'^2)}{5.5 \, c'^2 \sin(\theta/2)} - \frac{H_s \cot(\theta/2)}{3} - \frac{H_f (b' + c') t}{3c'^2} \tag{2.27}$$

Equation 2.9 expresses τ_{ihv}^{III} as a function of b, the half-diagonal length of the film/indenter contact area. From Figure 2.6(a) it can be seen that

$$b = \sqrt{2}\, b' \quad \text{and, likewise,} \quad c = \sqrt{2}\, c' \tag{2.28}$$

Applying this to equation 2.9, and using the relationship for H_f expressed in equation 2.21 for the moving indenter, yields the following result:

$$\tau_{ihv}^{III} = \frac{-0.6875 \, H_f}{\dfrac{k_1'(z)}{k_1(z)\phi} + \dfrac{\nu \, t}{\sqrt{2}\, b' \phi^2}} \tag{2.29}$$

where

$$H_f = \frac{W - 3H_s c'^2}{3(b'^2 - c'^2)}$$

$$c' = b' - t\tan(\theta/2)$$

$$\phi = \sqrt{\frac{6(1-\nu)}{(4+\nu)}} \qquad (2.30)$$

$$z = \frac{\sqrt{2}\, b'\phi}{t}$$

Similarly relating τ_{ihv}^{III} and τ_{ieff} to the total interfacial shear strength, τ_i, as was done for the leading edge orientation:

$$\tau_i = \tau_{ihv}^{III} + \tau_{ieff}$$

$$\Rightarrow \quad \tau_i = \left\{ \frac{-0.6875\, H_f}{\frac{k_1'(z)}{k_1(z)\phi} + \frac{\nu\, t}{\sqrt{2}\, b'\phi^2}} \right\} \qquad (2.31)$$

$$+ \left\{ \frac{F_h}{3c'^2} - \frac{\frac{2}{3}H_s}{5.5\sin(\theta/2)} - \frac{\frac{2}{3}H_f(b'^2 - c'^2)}{5.5\, c'^2 \sin(\theta/2)} - \frac{H_s\cot(\theta/2)}{3} - \frac{H_f(b'+c')t}{3c'^2} \right\}$$

C. SCRATCH TEST (CONICAL INDENTER)

In the following, the theoretical development for the use of a conical indenter in the constant-depth scratch test will be presented.

The modeling of a conical indenter is similar to that of a pyramidal indenter. Starting with the Ritter et al. [Refs. 1, 3] derivation of a spherical indenter:

$$\tau = \frac{\sigma_r}{\frac{k_1'(z)}{k_1(z)\phi} + \frac{\nu\, t}{a\phi^2}} \qquad (2.32)$$

The relationship between σ_r and H_f is $\sigma_r \approx -0.7222 H_f$ (see Appendix A). For Type II failure, the load W is supported by only the film (Figure 2.7):

$$W = H_f \pi b^2 \quad \Rightarrow \quad H_f = \frac{W}{\pi b^2} \tag{2.33}$$

Now equation 2.32 becomes:

$$\tau_{iv}^{II} = \frac{-0.7222\left[\frac{W}{\pi b^2}\right]}{\frac{k_1'(z)}{k_1(z)\phi} + \frac{\nu\, t}{b\phi^2}} \tag{2.34}$$

With Type III debonding, and W now being supported by both the film and the substrate as shown in Figure 2.7:

$$W = H_f A_f + H_s A_s = H_f \pi \left(b^2 - c^2\right) + H_s \pi c^2 \tag{2.35}$$

$$\Rightarrow \quad H_f = \frac{W - H_s \pi c^2}{\pi\left(b^2 - c^2\right)}$$

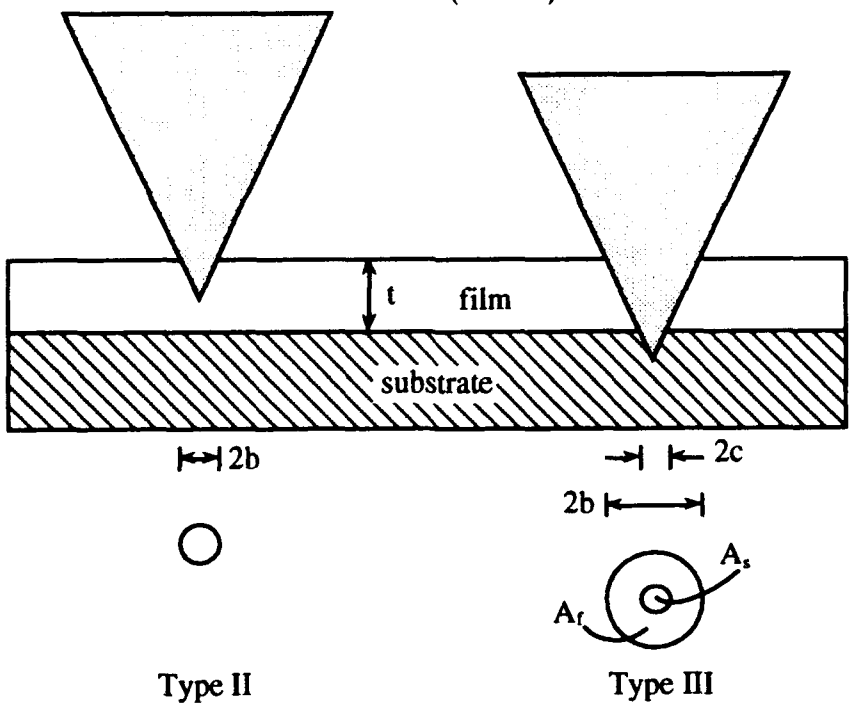

Figure 2.7: Geometry of Types II and II Debonding for Conical Indenter.

As with the pyramidal indenter, W is continuously measured during the test, b is measured using the Vicker's micro hardness tester measuring eyepiece, and c is known based on the geometry of the conical indenter. When the horizontal force is applied, and

the scratch is generated, only the front half of the indenter will be in contact with the film and substrate (Figure 2.8).

$$W = \tfrac{1}{2}\left[H_f \pi\left(b^2 - c^2\right) + H_s \pi c^2\right] \tag{2.36}$$

$$\Rightarrow \quad H_f = \frac{2W - H_s \pi c^2}{\pi\left(b^2 - c^2\right)}$$

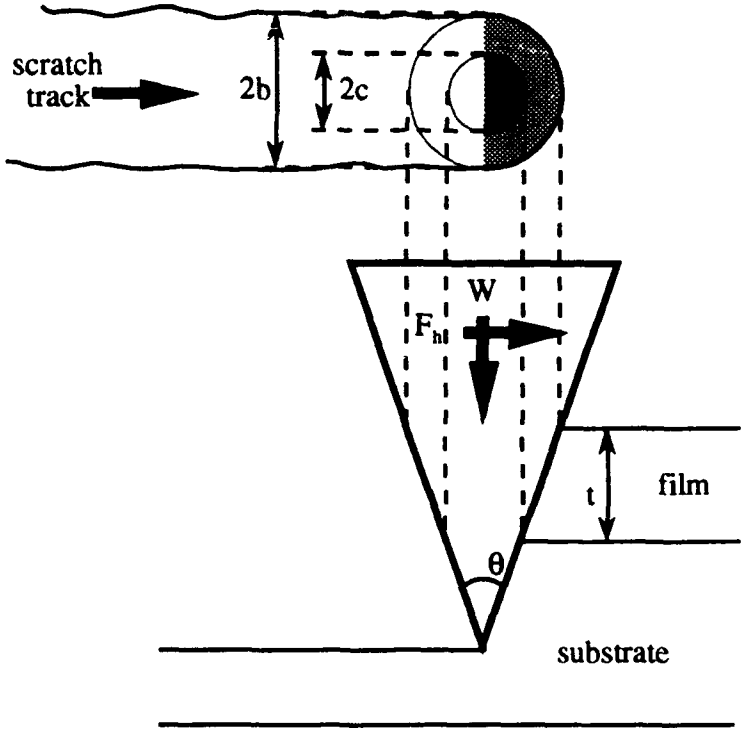

Figure 2.8: Projected Areas of Conical Indenter in Contact with Film and Substrate during Scratching.

Using equation 2.34, but using the value of H_f in equation 2.36, the Type III interfacial shear stress τ_{ihv}^{III} due to the normal load W and the applied horizontal force F_h is defined as:

$$\tau_{ihv}^{III} = \frac{-0.7222\left[\dfrac{2W - H_s \pi c^2}{\pi\left(b^2 - c^2\right)}\right]}{\dfrac{k_1'(z)}{k_1(z)\phi} + \dfrac{\nu\, t}{b\phi^2}} \tag{2.37}$$

where

$$c = b - t\tan(\psi/2)$$

$$\phi = \sqrt{\frac{6(1-\nu)}{(4+\nu)}} \tag{2.38}$$

$$z = \frac{b\,\phi}{t}$$

The application of the horizontal force must overcome the same opposing forces as determined by Benjamin and Weaver [Refs. 13, 21]. That is,

$$F_h = P_f + P_s + F_{s/ind} + F_{f/ind} + \tau_{ieff} A \tag{2.39}$$

where A is the area of the film-substrate interface.

The force to plough through the film P_f is:

$$P_f = AH_f = (b + c)t\,H_f \tag{2.40}$$

where A is the projected area in front of the cone in contact with the film.

The force to plough through the substrate P_s is:

$$P_s = AH_s = c^2\cot(\psi/2)\,H_s \tag{2.41}$$

where A is the projected area in front of the indenter in contact with the substrate.

The force to overcome the shear between the substrate and the indenter $F_{s/ind}$ is defined based on works be Benjamin and Weaver [Ref. 13] as:

$$F_{s/ind} = S_{s/ind} A \tag{2.42}$$

where $S_{s/ind}$ is the average shear strength of the substrate and A is the actual area of contact between the indenter and the substrate. Assuming that shear stresses exist only when there is material flow along the contact plane (the entire front half of the conical indenter) [Ref. 16], the incremental shear force dF acting on an area dA will be zero at the front of the indenter, and will be greatest at the sides of the indenter (see Figure 2.9). Since dF is a function of the angle γ between the front of the indenter and the particular dA in question:

$$dF = (S_{s/ind}\sin\gamma)(dA) \tag{2.43}$$

where dA is defined as (see Appendix B):

$$dA = \frac{r\, dr\, d\gamma}{\sin(\theta/2)} \tag{2.44}$$

Integrating both sides of equation 2.43, and dividing by the average angle γ, produces:

$$F_{s/ind} = \left[\frac{1}{\sin(\theta/2)} \right] \left[\frac{\iint \left(S_{s/ind}\, r \sin\gamma \right) dr\, d\gamma}{\int d\gamma} \right] \tag{2.45}$$

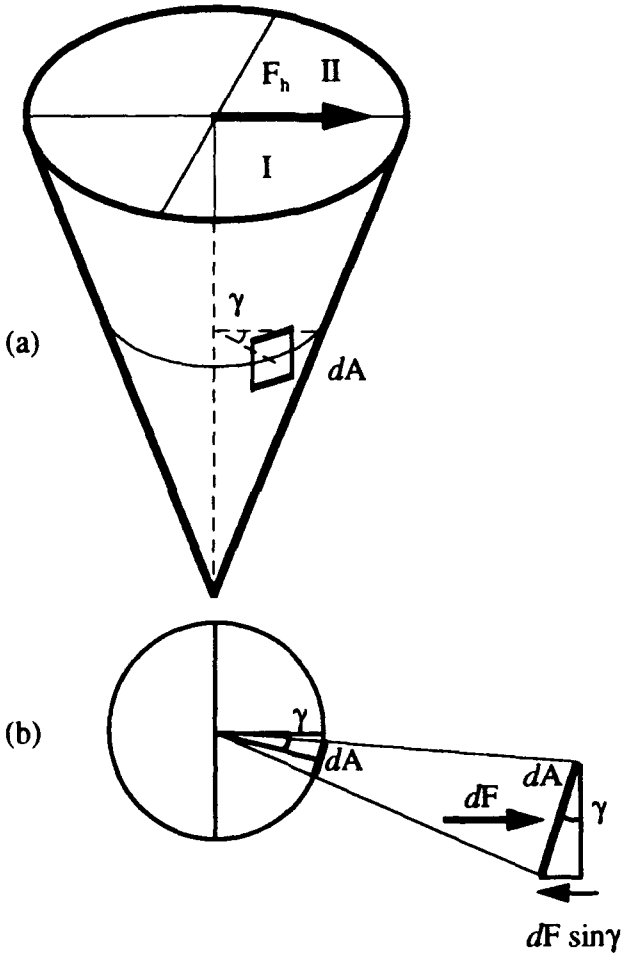

Figure 2.9: Resolution of Shear Forces: (a) Position of *d*A on Conical Indenter; (b) Top View of Conical Section Containing *d*A.

For simplicity, $F_{s/ind}$ will be determined in only quadrant I (Figure 2.9(a)), and then multiplied by 2. Knowing that $\theta=120^{o}$ for a Brale C indenter and that $S_{s/ind}=H_s/5.5$ (from equation 2.14), equation 2.45 reduces to:

$$F_{s/ind} = 0.4199\ H_s \left[\frac{\int_0^{\pi/2} \int_0^{c} (r \sin\gamma)\, dr\, d\gamma}{\int_0^{\pi/2} d\gamma} \right] \tag{2.46}$$

Evaluating the integral with respect to r yields:

$$F_{s/ind} = 0.4199\ H_s \left[\frac{\int_0^{\pi/2} \left[r^2/2 \right]_0^{c} \sin\gamma\, d\gamma}{\int_0^{\pi/2} d\gamma} \right] \tag{2.47}$$

Now equation 2.46 is:

$$F_{s/ind} = 0.2100\ H_s\ c^2 \left[\frac{\int_0^{\pi/2} \sin\gamma\, d\gamma}{\int_0^{\pi/2} d\gamma} \right] \tag{2.48}$$

Evaluating equation 2.48 with respect to γ produces:

$$F_{s/ind} = 0.2100\ H_s\ c^2 \left[\frac{[-\cos\gamma]_0^{\pi/2}}{[\gamma]_0^{\pi/2}} \right] = 0.2100\ H_s\ c^2 \left[\frac{1}{\pi/2} \right] \tag{2.49}$$

Therefore:

$$F_{s/ind} = 0.1337\ H_s\ c^2 \tag{2.50}$$

The force to overcome the shear between the film and the indenter $F_{f/ind}$ is derived similarly to $F_{s/ind}$, except the limits of r are now from c to b.

$$F_{f/ind} = S_{f/ind} A$$

$$\Rightarrow \quad dF = \left(S_{f/ind} \sin\gamma\right)(dA)$$

$$\Rightarrow \quad F_{f/ind} = \left[2/\sin(\theta/2) \right] \left[\frac{\int_0^{\pi/2} \int_c^{b} \left(S_{f/ind}\, r \sin\gamma\right) dr\, d\gamma}{\int_0^{\pi/2} d\gamma} \right] \tag{2.51}$$

where $S_{f/ind}=H_f/5.5$ (equation 2.14). Therefore:

$$F_{f/ind} = 0.1337\, H_f \left(b^2 - c^2\right) \tag{2.52}$$

The force to overcome the shear stress at the film-substrate interface F_{ieff} is:

$$F_{ieff} = \tau_{ieff} A = \tau_{ieff}\left(\pi c^2\right) \tag{2.53}$$

Combining the components of F_h in equation 2.39, solving for τ_{ieff}, and recalling that F_{ieff} is reduced due to the application of W, produces:

$$\tau_i = \tau_{ihv}^{III} + \tau_{ieff}$$

$$\Rightarrow \quad \tau_i = \left\{ \frac{-0.7222\, H_f}{\dfrac{k_1'(z)}{k_1(z)\phi} + \dfrac{\nu\, t}{b\phi^2}} \right\} \tag{2.54}$$

$$+ \left\{ \frac{F_h - H_f(b+c)t - H_s c^2 \cot(\varphi/2) - 0.1337\, H_s c^2 - 0.1337\, H_f \left(b^2 - c^2\right)}{\pi c^2} \right\}$$

It should be noted that while the tip radius of a Vicker's indenter will be less than a micron [Ref. 16], the tip of a conical indenter may vary from 25μ-200μ. This is significant when considering the film thickness t of the sample being tested. There exists a minimum penetration p_{min} such that for any value less than p_{min}, the conical indenter will behave as, and should then be modeled as, a spherical indenter. See Figure 2.10.

$$\begin{aligned} p_{min} &= R - R\cos\varphi \\ &= R(1 - \cos\varphi) \\ &= R\left[1 - \cos(90 - (\varphi/2))\right] \end{aligned} \tag{2.55}$$

By geometry, an indentation of p_{min} will correspond to a half-track width b of:

$$b = R\sin\varphi = R\cos(\varphi/2) \tag{2.56}$$

For a commercial Brale C conical indenter with an apex angle of 120° and a tip radius of 200μ, p_{min}=0.134R=26.8μ and b=100μ. With this indenter, for Type III debonding to

occur, and assuming a minimum penetration into the substrate, the film thickness will need to be at least 26.8μ. Therefore, the Brale indenter is suitable as a conical indenter only for film thicknesses considerably larger than 26.8μ.

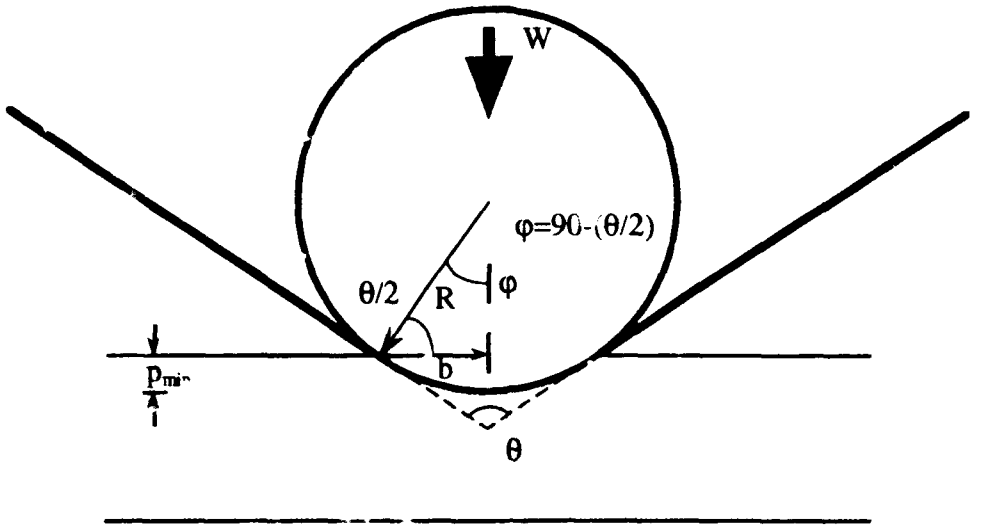

Figure 2.10: Relationship between p_{min} and Indenter Tip Radius.

III. EXPERIMENTAL

A. OVERVIEW

A vertical load is applied to a film-substrate pair (which undergoes Type III indentation debonding) with a Vicker's indenter such that the entire film and part of the substrate are penetrated. The vertical load is just less than that required for Type III debonding. Once the entire film is penetrated, the depth of penetration of the indenter is kept fixed. A horizontal force is then applied to generate a scratch. The vertical and horizontal forces are monitored continuously during the scratching process, and the data is stored via the data acquisition computer for future use.

After the scratch has been generated, the sample is observed under the Vicker's micro hardness tester microscope. The maximum width of the scratch track ($2b_{max}$) and minimum width ($2b_{min}$) are noted at several locations along the track.

The film-substrate interfacial shear strength can be calculated knowing the following parameters: horizontal force, vertical force, maximum and minimum track widths, film thickness, fil.. Poisson's ratio, and substrate indentation hardness.

B. APPLICATION OF THEORETICAL MODEL

1. Area of Forward Lateral flaking

Figure 3.1 illustrates a scratch through a chromium-on-glass sample. This was compared to diagrams by Hedenqvist et al. (Figure 1.5) and Bull (Figure 1.6). In both cases, a failure mode of either forward lateral flaking (FLF) or spallation ahead of the indenter appears to be prevailing. Hedenqvist describes the cause of FLF to be the result of compressive stresses building up in front of the indenter, and causing the film to buckle

and be removed in semi-circular flakes. Another failure mode is sideward lateral flaking (SLF). The end result of FLF and SLF damage appears similar, but *in situ* monitoring permits one to observe if the flakes break away from the front or side of the indenter [Ref. 19]. Bull's work, which is more recent, does not address whether the spallation originates from the front or side of the indenter [Ref. 20]. The assumption will be made for this thesis that FLF occurred.

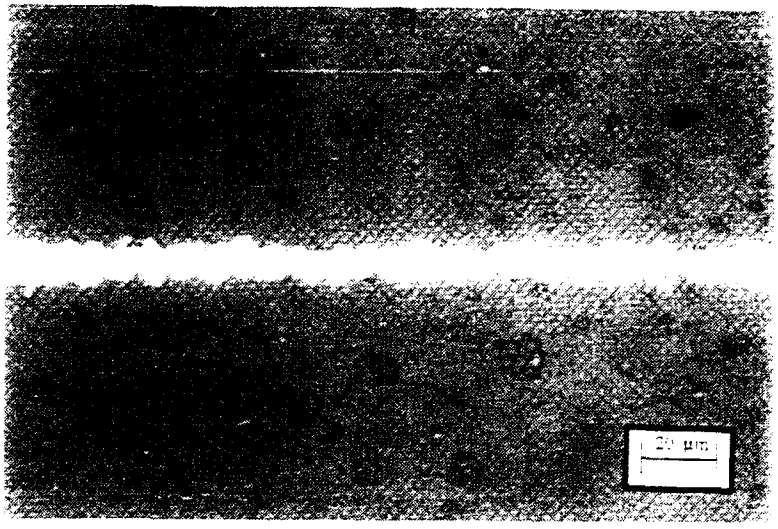

Figure 3.1: Chromium on Glass Displaying Characteristics of Forward Lateral Flaking, Film Thickness 0.1μ (500x).

The areas of flake removal in front of the indenter appear to be more circular than semicircular. The scratch track in Figure 3.1 can therefore be modeled as shown in Figure 3.2. The effects of this are two-fold.

First, since a circular region of coating has been removed in front of the indenter, the sides of the indenter will not be in contact with the film as the scratch is generated. There will be no film material flow past the sides of the indenter; therefore, there will be no shear between the film and the indenter. The components of the horizontal force F_h now become:

$$F_h = P_f + P_s + F_{s/ind} + \bar{\tau}_{ieff} A \qquad (3.1)$$

Second, the term $\bar{\tau}_{ieff}A$ represents the average force to overcome the shear between the film and substrate of the area over which the film was removed; that is, the circular area in front of the indenter. This area A_{FLF} is defined as (see Appendix C):

$$A_{FLF} = \pi\, b_{max}^2 - b_{max}^2 \sin^{-1}\left(b_{min}/b_{max}\right) + b_{min} b_{max} \cos\left[\sin^{-1}\left(b_{min}/b_{max}\right)\right] \qquad (3.2)$$

where b_{min} and b_{max} are illustrated in Figure 3.2. Equation 3.1 now becomes:

$$F_h = P_f + P_s + F_{s/ind} + \bar{\tau}_{ieff} A_{FLF} \qquad (3.3)$$

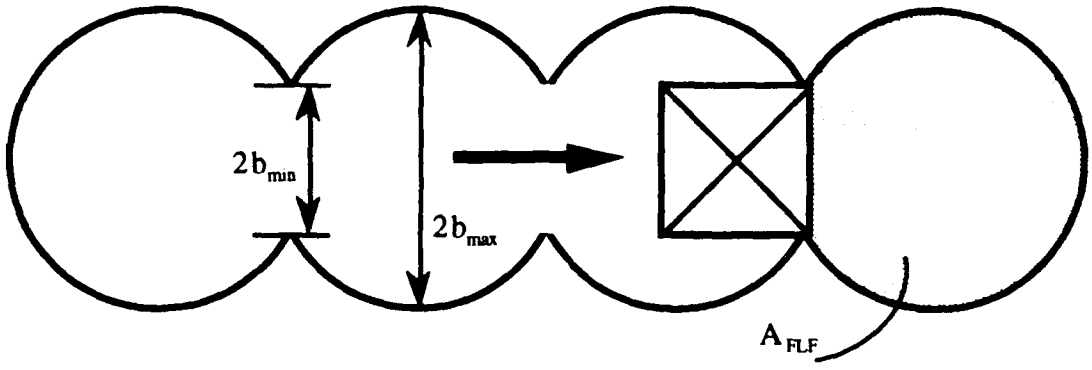

Figure 3.2: Forward Lateral Flaking Model.

Solving for $\bar{\tau}_{ieff}$ and using the relationships of equations 2.21, 2.22, 2.23, and 2.25 yields:

$$\bar{\tau}_{ieff} = \frac{F_h - \dfrac{2c^2 H_s}{5.5 \sin(\theta/2)} - c^2 H_s \cot(\theta/2) - H_f (b_{min} + c)t}{\pi\, b_{max}^2 - b_{max}^2 \sin^{-1}\left(b_{min}/b_{max}\right) + b_{min} b_{max} \cos\left[\sin^{-1}\left(b_{min}/b_{max}\right)\right]} \qquad (3.4)$$

2. τ_{lhv}^{III} Determination

Ritter's derivation [Ref. 2] of the equation to determine the interfacial shear stress (equation 2.1) was based on the critical load P_c to cause debonding at the perimeter of the contact zone. Matthewson [Ref. 1] had previously determined that this was the region of

maximum interfacial shear stress. For regions outside the perimeter of contact, the interfacial shear was a function of the distance r from the contact perimeter [Ref. 3].

In equation 2.31 the contribution of τ_{ihv}^{III} to τ_i is that value of τ_{ihv}^{III} determined at the film-indenter contact radius. Mathematically, though, this value of τ_{ihv}^{III} should be a function of the variable r, which is evaluated over an area that is also dependent on the variable r. The average interfacial shear stress over the flake area due to the vertical indentation can therefore be expressed as:

$$\bar{\tau}_{ihv}^{III}(r) = \frac{\int \tau(r)\, dA}{\int dA} \tag{3.5}$$

The denominator is simply the area over which $\bar{\tau}_{ihv}^{III}$ acts; that is, A_{FLF}. The numerator can be rewritten, using polar coordinates, in the following manner:

$$\iint \tau(r)\, r\, dr\, d\lambda \tag{3.6}$$

The geometry of this situation requires the determination of the area of a partial circle which is offset from the origin of the coordinate system (Figure 3.3(a)). Momentarily ignoring the protrusion of the indenter into the circle, Figure 3.3(b) is a geometric representation of the circular shaped region of FLF material removal. The equation of this circle is [Ref. 23]:

$$b^2 = d^2 + r^2 - 2\, r\, d \cos(\lambda - \beta) \tag{3.7}$$

For simplicity, let β=0 and redefine b to be b_{max} (as in Figure 3.2). Equation 3.7 is now:

$$b_{max}^2 = m^2 + r^2 - 2\, m\, r \cos\lambda \tag{3.8}$$

with remaining factors shown in Figure 3.3(c). By geometry:

$$m = b_{min} + b_{max} \cos\alpha \quad \text{and} \quad \alpha = \sin^{-1}\left(b_{min}/b_{max}\right) \tag{3.9}$$

Solving for r:

$$r = m \cos\lambda \pm \sqrt{m^2 \cos^2\lambda - m^2 + b_{max}^2} \tag{3.10}$$

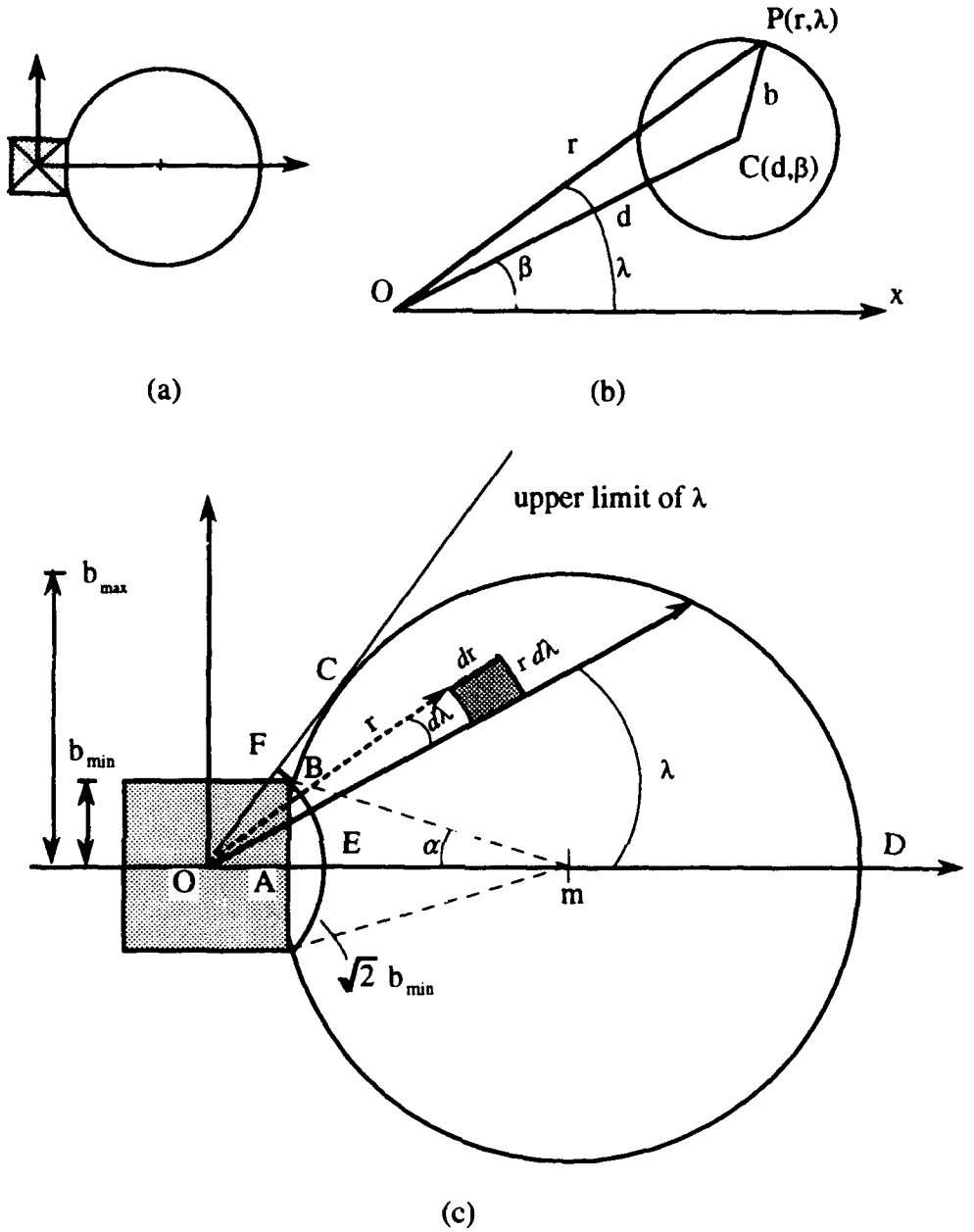

Figure 3.3: Geometry of Film Removal in Front of Indenter: (a) Circular Region in Front of Indenter; (b) Model of Offset Circle; (c) Parameters Used in Calculations.

The area desired is twice that enclosed by points ABCDA. However, to simplify this model, the area enclosed by points EFCDE will be considered. This alleviates the complexity of the geometry by avoiding the combination of polar and rectangular

coordinate systems. For purposes of this model, the difference in area can be ignored. This simplification produces the following limits of integration:

$$r = \sqrt{2}\, b_{min} \text{ to } m\cos\lambda + \sqrt{m^2\cos^2\lambda - m^2 + b_{max}^2}$$

$$\lambda = 0 \text{ to } \sin^{-1}\left(b_{max}/m\right) \tag{3.11}$$

The double integral will be multiplied by 2 to account for the bottom half of A_{FLF}. Substituting the variable r for b_{min} in the τ_{ihv}^{III} contribution of equation 2.31:

$$\tau(r) = \frac{-0.6875\, H_f}{\dfrac{k_1'\left(r\phi/t\right)}{k_1\left(r\phi/t\right)\phi} + \dfrac{\nu\, t}{r\phi^2}} \tag{3.12}$$

The film indentation hardness H_f is not integrated over the area of flake removal. H_f is a function of only the area of film supporting the load imposed by the Vicker's indenter. z has been represented by the relationship in equation 2.2. $k_1(z)$, a modified Bessel function of the second kind, and its derivative with respect to z, $k_1'(z)$, are carried out to three terms each (see Appendix F). Substituting these expanded functions results in τ_{ihv}^{III} being expressed as a function of the variable r:

$$\tau(r) = \frac{-0.6875\, H_f}{\dfrac{-\left[1 + \dfrac{(\mu+3)t}{8\,r\,\phi} + \dfrac{(\mu-1)(\mu+15)t^2}{128\,r^2\,\phi^2}\right]}{\left[1 + \dfrac{(\mu-1)t}{8\,r\,\phi} + \dfrac{(\mu-1)(\mu-9)t^2}{128\,r^2\,\phi^2}\right]\phi} + \dfrac{\nu\, t}{r\phi^2}} \tag{3.13}$$

where μ=4 for the modified Bessel function of the second kind. Rearranging equation 3.13, inserting it into equation 3.5, and applying the limits of 3.11 results in the following expression for the average interfacial shear stress due to the vertical load only over the flake area:

$$\bar{\tau}(r)_{ihv}^{III} = \frac{2}{A_{FLF}} \int_{\lambda=0}^{\sin^{-1}\left(b_{max}/m\right)} \int_{r=\sqrt{2}\,b_{min}}^{m\cos\lambda+\sqrt{m^2\cos^2\lambda-m^2+b_{max}^2}} \left[\frac{-0.6875\, H_f \left(1+\frac{3t}{8r\phi}+\frac{-15t^2}{128\,r^2\phi^2}\right) r^2\phi^2}{-r\phi\left(1+\frac{7t}{8r\phi}+\frac{57t^2}{128\,r^2\phi^2}\right)+\nu\, t\left(1+\frac{3t}{8r\phi}+\frac{-15t^2}{128\,r^2\phi^2}\right)} \right] dr\, d\lambda$$

(3.14)

This ponderous integral is solved numerically [Refs. 24, 25] using Simpson's Rule with eight intervals. The value of $\bar{\tau}_{ihv}{}^{III}$ obtained is added to $\bar{\tau}_{ieff}$ as was done in equation 2.31 to produce the total interfacial shear strength, $\bar{\tau}_i$:

$$\bar{\tau}_i = \bar{\tau}_{ihv}^{III} + \bar{\tau}_{ieff}$$

$$= \underbrace{\frac{\int \tau(r)\, dA}{\int dA}}_{\text{(eqn 3.14)}} + \underbrace{\bar{\tau}_{ieff}}_{\text{(eqn 3.4)}} \qquad \textbf{(3.15)}$$

The program module for the numerical integration is listed in lines 2510 through 3030 of the computer program in Appendix E.

C. APPARATUS

Figures 3.4 and 3.5 illustrate the experimental apparatus.

The scratch generating apparatus is mounted on an Instron testing machine. The rigidity of the testing machine eliminates any vertical relative motion between the indenter and sample, thereby ensuring a constant scratch depth is maintained. The Vicker's indenter is mounted to the movable crosshead, which is used to place a previously determined load on the indenter against the specimen. A load cell between the indenter and the crosshead provides continuous vertical load data.

The sample is mounted to the translation table with screw-down clamps. The table is supported by two 1/2 inch stainless steel rollers. The horizontal force cell, providing continuous horizontal force data, is rigidly mounted on the edge of the table. A DC

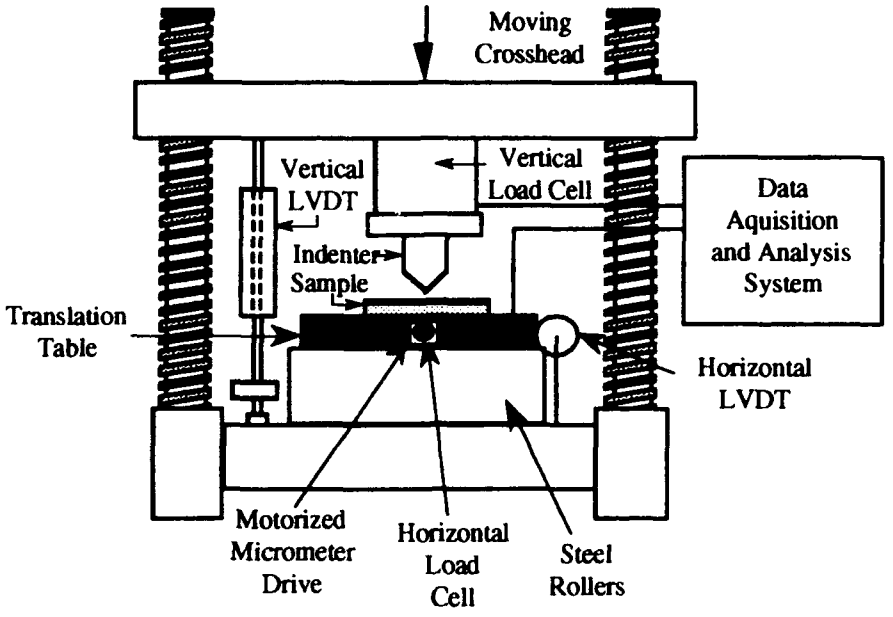

Figure 3.4: Scratch Apparatus Overview.

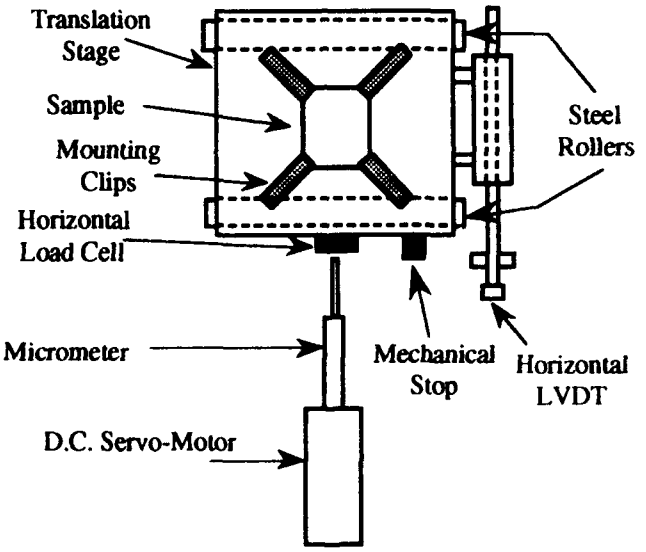

Figure 3.5: Detail of Motorized Translation Table.

motor-driven micrometer pushes against the load cell causing the table to roll beneath the indenter. The thin wire cabling from the horizontal load cell is positioned from the table at 90^{o} to the table's motion. This ensures a slight positive force is applied to the table; therefore, the table and load cell are always in contact with the micrometer head. The start

and finish positions of the micrometer are used in conjunction with the time duration of the test to determine positions of the table during the scratch.

A Hewlett-Packard 3852A Data Acquisition/Control Unit (DAQ) collects and monitors the output readings of the two load cells. An IBM computer drives the DAQ, converts the voltage readings to force readings, and calculates the interfacial shear strength based on the two forces and user-inputted parameters. The programs and algorithms for collecting and analyzing the data, written in IBM-BASIC, are provided as Appendices D and E.

D. PROCEDURE

1. Sample Preparation

a. Copper/Glass Samples

Copper/glass samples were prepared by Covac Vacuum Services of Livermore, California. Microscope glass slides, provided to Covac, were cleaned with an Alconox solution, followed by a 200 proof alcohol rinse, and then dried with nitrogen gas. The slides were placed in a vacuum chamber which was evacuated to $1x10^{-5}$ torr. After backfilling the chamber with argon gas to $5x10^{-3}$ torr, the slides were sputtered with argon ions for five minutes at 500 VDC and 500 mA. The glass slides were then sputtered coated with 99.99% copper to thicknesses of 0.1μ, 0.2μ, 0.3μ, 0.4μ, and 0.5μ. The evaporation process was conducted at $2x10^{-3}$ torr, 500 VDC, and 600 mA. Completed samples were stored in an evacuated dessicator. [Ref. 15]

b. Chromium/Glass Samples

Chromium/glass samples were prepared on site. Microscope glass slides were initially cleaned with an all-purpose cleaner to remove any grease residue. The slides were then cleaned in a 40% nitric acid solution, followed by a distilled water rinse. The water was displaced by 190 proof alcohol, and the slides then dried with hot air. The slides were placed in a vacuum chamber which was evacuated to $2x10^{-7}$ torr. 99.9%

chromium was evaporated onto the slides to various thicknesses of 0.1μ to 0.4μ. The evaporation process was conducted at $1x10^{-6}$ torr and 35-45 A. Completed samples were stored in an evacuated dessicator.

2. Scratch Test Procedure

a. *Preliminary Data*

The computer program used to analyze the experimental data requires some preliminary information to be determined prior to the actual scratch test. The substrate indentation hardness H_s was determined by Ritter et al. The value used was 557.7 kg/mm^2 [Ref. 9].

Prior to scratching a sample with a known film thickness, several Vicker's hardness tests at varying loads were conducted. This determined the load to cause Type III debonding at the film-substrate interface. This load, when applied during the scratch test, ensured the film was removed along the scratch track.

Due to imperfections in the translation table (such as the flexibility of the horizontal load cell wiring), the force required to push the table without vertical loading of the Vicker's indenter was not constant. Comparing the horizontal force data from two runs without vertical loading enabled one to verify the horizontal force fluctuations due to these imperfections were at least consistent between consecutive runs. Therefore, two sets of data were obtained, and then averaged to establish a nominal baseline of horizontal force data. The sample was sprayed with a light coat of a petroleum-based lubricant, such as WD-40, and then placed on the translation table. The lubricant sealed out moisture and airborne contaminants, thereby improving the repeatability of the testing. The indenter was not lowered. The micrometer motor was energized, and the table was pushed a known distance at a nominal speed of 7.7 μ/sec. The horizontal force to push the table was measured and stored in a BASE'A' data file for future use. At the conclusion of the run, the motor was reversed, and the table was allowed to return to its original position. The

return to the starting position was accomplished due to the previously described positive force between the load cell and the micrometer head. Without making any physical adjustments to the apparatus, a second baseline data run was conducted. Again, the force to push the table was measured and stored in a BASE'B' data file. The table and micrometer head were then returned to the original starting position.

b. Real Time Data Acquisition

Following the two baseline data runs, the Instron crosshead with the indenter was manually lowered via the screw drive and gear assemblies. While the vertical load cell output voltage was being observed on the DAQ, the indenter was lowered onto the sample until the output voltage corresponded to a load just less than that previously determined to produce Type III indentation debonding in the given sample. The micrometer motor was energized, and the translation table was pushed at the same speed and for the same distance as during the baseline data runs. The vertical and horizontal load cells output voltages were measured and stored in a RESULT data file. The sample was removed from the scratch test apparatus and placed on the Vicker's micro hardness tester. Using the measuring eyepiece, the maximum and minimum track widths, b_{max} and b_{min}, were measured at various points along the scratch track to obtain representative values of b_{max} and b_{min}.

3. Data Analysis

The two BASE data files were observed with a graphics program to verify the repeatability of the measured horizontal force between the two baseline data runs. Figure 3.6(a) demonstrates this repeatability for two nominal runs. In this case, the average of the two horizontal load cell outputs in the BASE data files was subtracted from the horizontal load cell output of the RESULT data file to obtain the net horizontal force F_h required to produce the scratch on the specimen. The translation table was initially resting against a mechanical stop. When the motor-driven micrometer was energized, the

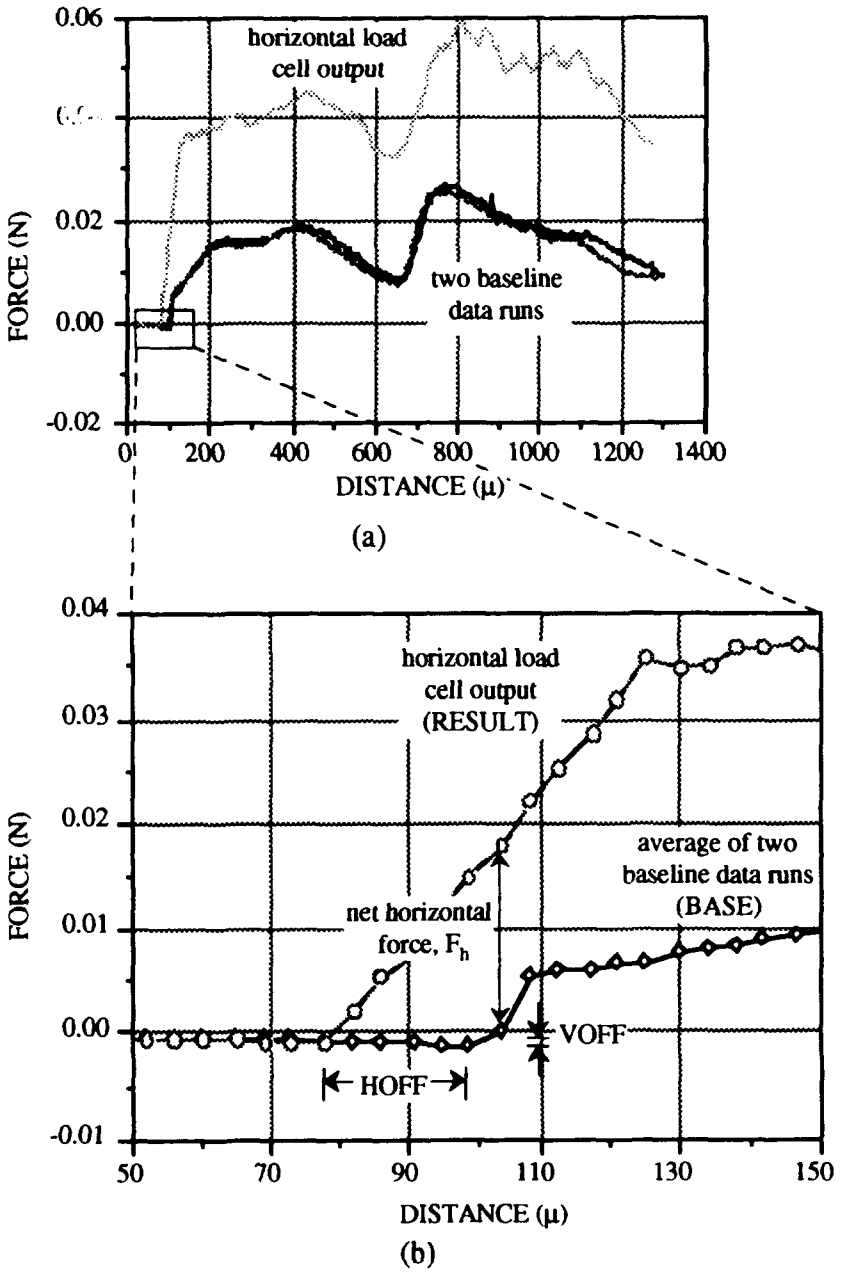

Figure 3.6: Horizontal Force Determination: (a) Verifying Repeatability between Two Baseline Runs; (b) Determining HOFF and VOFF.

horizontal load cell sensed no load until the micrometer advanced enough to push the table away from the stop (Figure 3.5). Since the data acquisition system was started manually before the micrometer pushed against the load cell, the exact moment (zero reference) when

the load cell sensed the table being pushed away from the stop may have varied between adjacent runs. The result was a horizontal offset (HOFF) of the zero reference between RESULT and BASE data. Likewise, any difference in the no-load voltage of the horizontal load cell may have resulted in a vertical offset (VOFF) of the zero reference between RESULT and BASE data. Ensuring the zero references between runs was coincident was necessary so that the difference between a given set of RESULT and BASE data points was the net horizontal force F_h for that point. The values of HOFF and VOFF were determined by observation of the horizontal force plots. See Figure 3.6(b).

The results of the scratch track were analyzed using the EVALUAT program. The program prompts the user for the scratch test data and material properties of the film and substrate. The shear stress due to the vertical load (τ_{ihv}^{III}), the average shear stress due to the horizontal load ($\bar{\tau}_{ieff}$), and the mean interfacial shear (τ_i) were then calculated. Problems were encountered in calculating the mean value $\bar{\tau}_{ihv}^{III}$ as per equation 3.14, and so the reported values represent τ_{ihv}^{III} (equation 2.29), and not $\bar{\tau}_{ihv}^{III}$.

E. RESULTS

Initially, samples used for the scratch test consisted of copper films on microscope slide glass. Copper was chosen for its ductility and applications in electronics. Figure 3.7 illustrates two Vicker's indentations on such a sample. The ridge surrounding the pyramidal indentation indicates debonding at the interface. This was noted before the load was sufficient to cause plastic deformation of the substrate. The plastic deformation of the copper film accompanied by interfacial debonding without substrate penetration is characteristic of Type II failure. Since this scratch test requires the Vicker's indenter to be loaded to just less than that which would cause Type III debonding, a new film-substrate system was chosen. A chromium film was selected since it adheres well to glass, although it is more brittle compared to a copper film. Figure 3.8 illustrates an indentation on a

chromium-on-glass sample. The same load as that applied to the copper sample was applied to the chromium sample; no debonding was noted. At slightly higher loads, the film was fully penetrated; again, no debonding occurred. This indicated that chromium-on-glass was suitable for this scratch test.

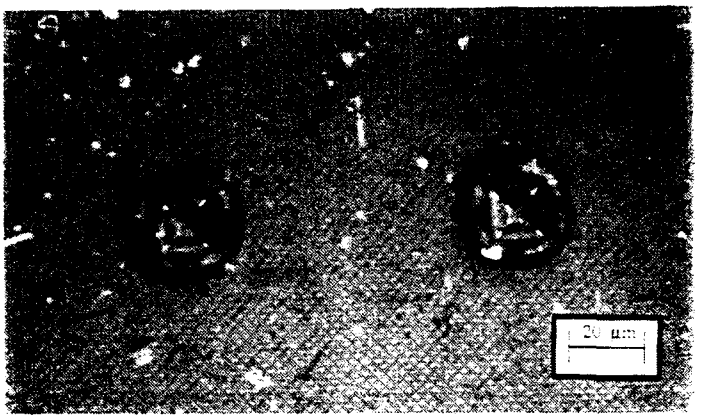

Figure 3.7: Vicker's Indentation, Copper on Glass, Film Thickness 0.37µ, Normal Load 12 Grams (500x).

Figure 3.8: Vicker's Indentation, Chromium on Glass, Film Thickness 0.10µ, Normal Load 20 Grams (500x).

Two tests were conducted on two chromium-on-glass samples. In the first test, an initial indenter load of 32 grams was applied to a sample with a film thickness of 0.33µ. The nominal interfacial shear strength τ_i was 205 MPa. For the second test, an initial load of 21 grams was applied to a sample with a film thickness of 0.27µ. The resultant τ_i was

199 MPa. For both these tests, the initial load was greater than that for complete penetration of the film, but less than that to cause Type III debonding. Figure 3.9 shows the scratch channels for these two tests. The faint trace down the center of each channel indicates the occurrence of substrate plastic deformation. This confirms the initial normal load was adequate for completely penetrating the film. The measured normal load W and

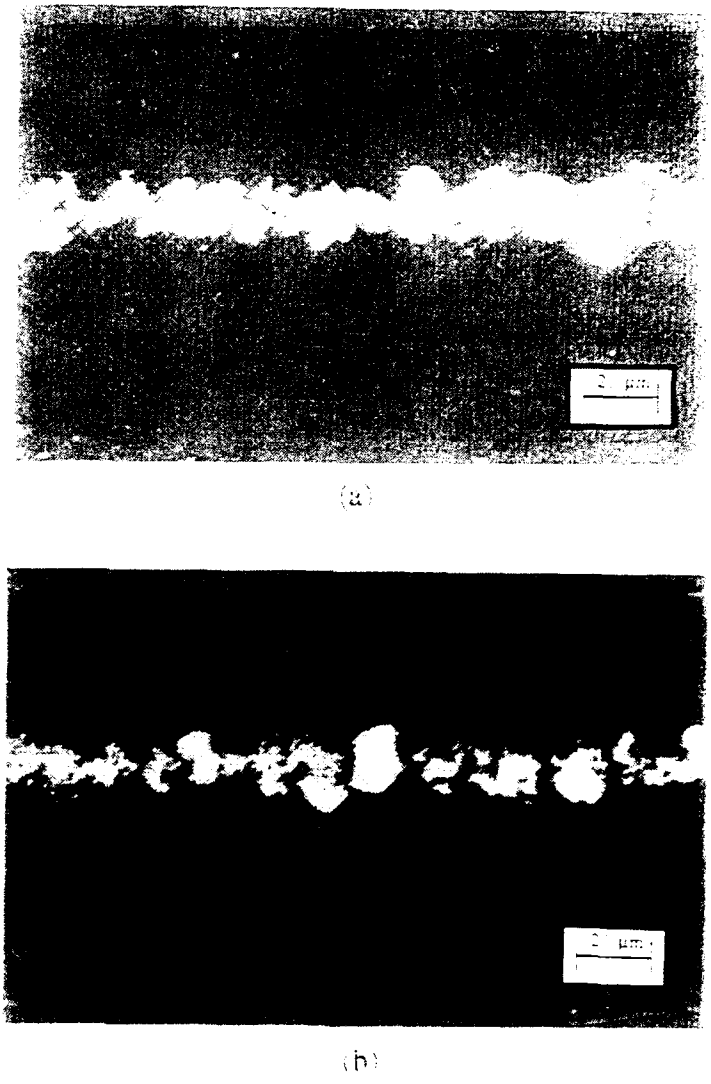

Figure 3.9: Scratch Channels for Chromium-on-Glass Samples: (a) Film Thickness 0.33μ, Initial Indenter Load 32 Grams (500x); (b) Film Thickness 0.27μ, Initial Indenter Load 21 Grams (500x).

the applied horizontal load F_h, as well as the calculated shear strengths (τ_{thv}^{III}, $\bar{\tau}_{ieff}$, and τ_i) are displayed in Figures 3.10 and 3.11. The characteristic circular flake formation of forward lateral flaking is evident in both test, although it is not a pronounced as that on the sample with a substantially thinner film displayed in Figure 3.1.

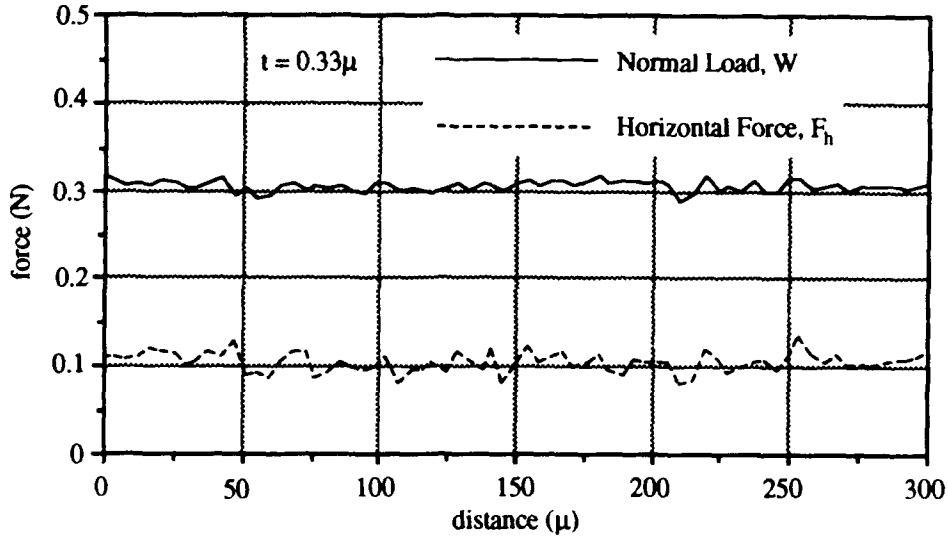

(a)

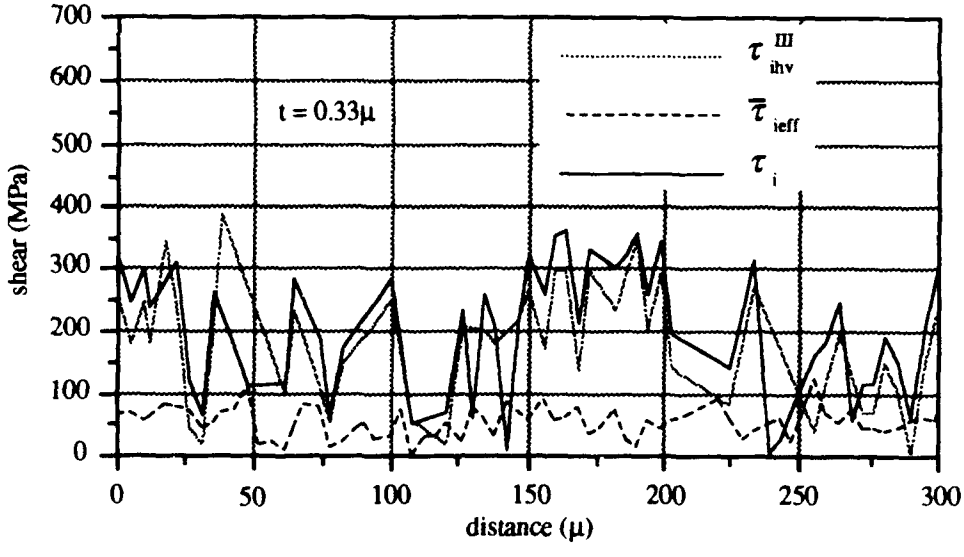

(b)

Figure 3.10: Results of Chromium-on-Glass Scratch Test, Film Thickness 0.33μ: (a) Measured Forces; (b) Calculated Shear Strengths.

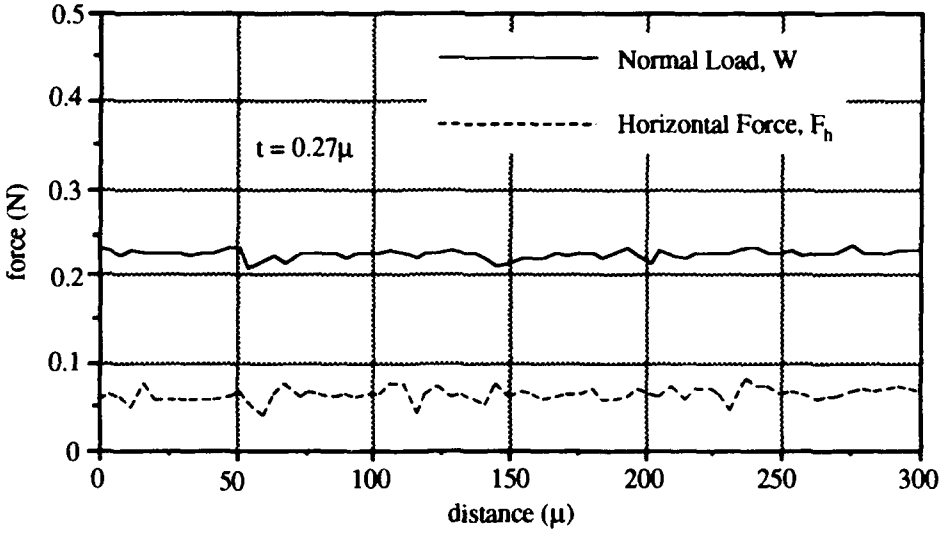

(a)

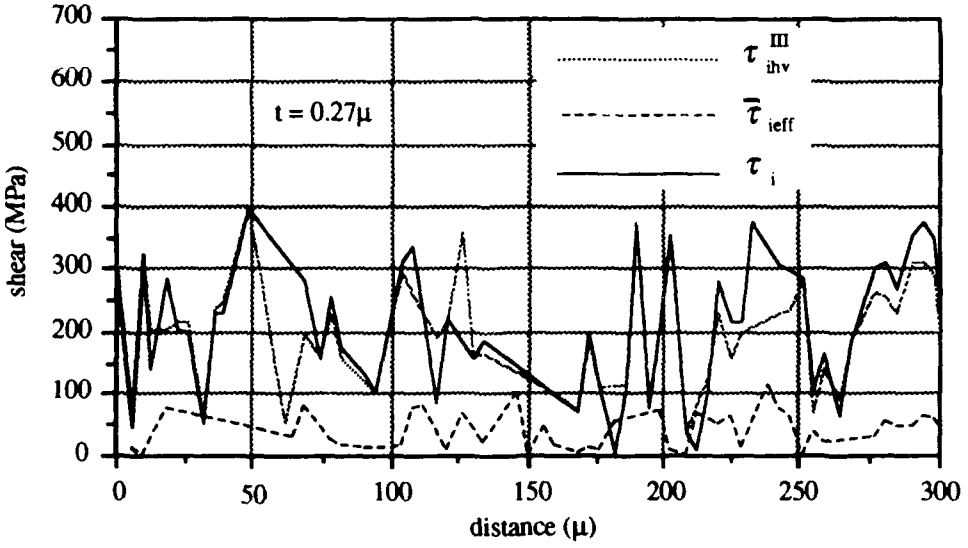

(b)

Figure 3.11: Results of Chromium-on-Glass Scratch Test, Film Thickness 0.27μ: (a) Measured Forces; (b) Calculated Shear Strengths.

IV. CONCLUSIONS / RECOMMENDATIONS

The use of the constant-depth scratch test has produced results that are reasonable in comparison with those using other methods. Works by Valli et al. [Ref. 11, 17] and Sekler [Ref. 18] indicated the necessity of using acoustic emissions in conjunction with force measurements to detect failure of the interfacial bond. However, by maintaining the constant depth of the indenter after Type III failure has already been established, in combination with the use of extremely sensitive load cells, this requirement has been removed. Any error due to an ambiguous estimate of the moment of interfacial failure has been eliminated. Additionally, the complexity of the apparatus to conduct the scratch test has been reduced considerably.

The derivation of a general equation for determining τ_i (equation 2.20 for leading edge Vicker's indenter, equation 2.31 for leading plane Vicker's indenter or equation 2.54 for conical indenter) does not account for any damage mechanisms. For any given film-substrate system, the results of a preliminary scratch test (using a general equation) should be analyzed under a microscope for patterns of different failure modes. If a mode is present, a theoretical model should be formulated, and the general equation modified appropriately. The same procedure would apply for a change in indenter for the same film-substrate system.

Since the primary interest for this thesis is in the area of electronics, scratch tests should be conducted on film-substrate systems applicable to this area. Film-substrate combinations would be copper on aluminum nitride (AlN) or gold on AlN. Due to the complications arising from determining the exact moment of interface failure for a

non-transparent substrate when using an indentation or conventional scratch test, the opaqueness of this AlN substrate should reinforce the simplicity of this scratch tester.

Testing with the conical indenter and its general equation (equation 2.54) to calculate the interfacial shear strength has not been conducted. By using the same film-substrate system as that used for the Vicker's indenter, a comparison of obtained τ_i values can be made. Influences due to any failure modes observed need to be incorporated into the general equation.

As shown by Matthewson [Ref. 3], the interfacial shear stress should decrease as the distance from the contact radius increases. However, arbitrarily substituting increasing values of r into equation 3.13 resulted in an increase of $\tau(r)$. The increase was relatively insignificant; however, it indicated that Ritter's equation for interfacial shear stress (equation 2.1) might have been incorrectly applied in this thesis for deriving the shear stress at some distance beyond the contact radius. The use of this equation needs to be further investigated.

The measurement of the horizontal force using the baseline subtraction method is an effective alternative to dealing with inconsistencies of the translation table as long as all present force fluctuations can be detected. The load cell currently in use is being operated within the lower 2-5% of its range. A load cell of capacity such that detected loads will fall within 10-90% of the range should be installed.

A more advanced solution would incorporate both the horizontal and vertical load cells into one multiple-component load cell to which the Vicker's indenter is mounted. By moving the sample underneath the indenter, and measuring the horizontal force this imparts to the indenter, any contributions due to the friction effects of the table would be isolated from the load cells.

The table on rollers is a modification to overcome the "stiction" effects (skipping and jumping due to increased forces required to initiate movement). While this problem was

solved, the low friction between the aluminum table and steel rollers can allow for motion perpendicular to the scratch direction in the horizontal plane, a deviation not considered in the model. A more refined roller table is needed.

An overall re-design of the test apparatus should be considered. The above recommendations are addressing specific problems with the equipment. However, the remedy for one problem may create, or accentuate, another one. For example, the steel rollers significantly reduced the stiction effects, but the introduction of the second degree of freedom in the horizontal plane of the table led to the stiffness of the horizontal load cell wiring affecting the horizontal force measurement. One possibility is the acquisition of a commercial scratch tester, which would then be modified to meet the constant-depth requirement.

APPENDIX A - THE RELATIONSHIP BETWEEN RADIAL STRESS AND INDENTATION HARDNESS

A. VICKER'S INDENTER

In the use of the Vicker's indenter for determining the hardness of a material, the indentation pressure, P_i, is defined as:

$$P_i = \frac{\text{load}}{\text{projected area}} = \frac{W}{(L/\sqrt{2})^2} = \frac{2W}{L^2} \qquad \textbf{(A.1)}$$

where W is the applied load and L is the length of the diagonal of the indentation. Works by Bowden and Tabor (Figure A.1) [Ref. 22] relating the yield pressure, P_m, to the elastic limit, Y, indicate that for a pyramidal indenter of half-angle 68°, there exists the relationship:

$$P_m = 3.2Y \qquad \textbf{(A.2)}$$

By applying Tresca's flow criteria [Ref. 15],

$$\sigma_{max} - \sigma_{min} = Y \qquad \textbf{(A.3)}$$

where σ_{max} is P_i and σ_{min} is the compressive radial stress, σ_r. In the application of the scratch test, the indenter load is just that that will cause Type II failure of the film-substrate interface. That is, the indenter has caused plastic deformation of the film, and the maximum stress is the yield pressure, or the indentation pressure. Equation A.3 is now:

$$P_i - (-\sigma_r) = Y \;\Rightarrow\; \sigma_r = Y - P_i \qquad \textbf{(A.4)}$$

Using equation A.2,

$$\sigma_r = \frac{P_i}{3.2} - P_i = -0.6875P_i \qquad \textbf{(A.5)}$$

In Bowden and Tabor it is shown that P_i is independent of the applied load, whether or not the material work hardens under the load. Therefore, P_i is equal to the indentation hardness, H_f, and

$$\sigma_r = -0.6875H_f \qquad \textbf{(A.6)}$$

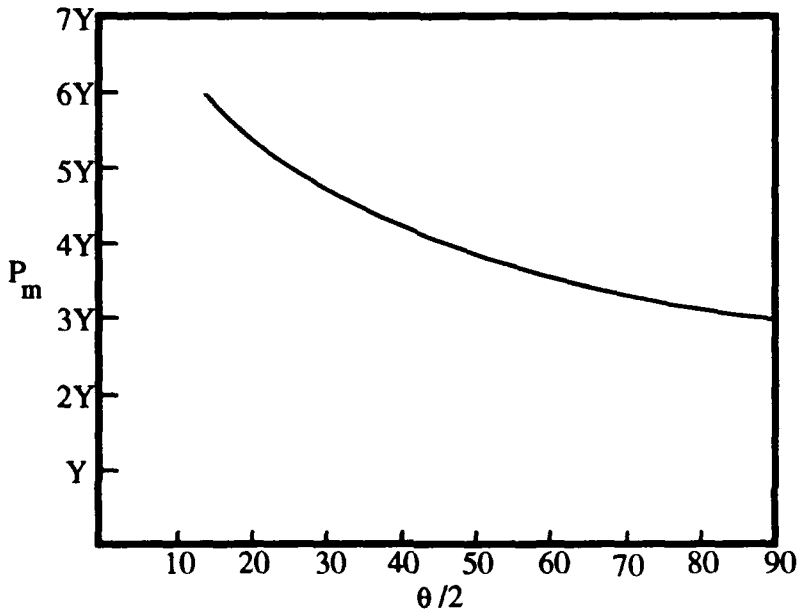

Figure A.1: Yield Pressure as a Function of Semi-Angle [Ref. 22].

B. CONICAL INDENTER

The relationship between the radial stress and the indentation hardness for the use of a conical indenter is derived similarly to that of the Vicker's indenter. The indentation pressure, P_i, is:

$$P_i = \frac{\text{load}}{\text{projected area}} = \frac{W}{\pi b^2} \qquad \textbf{(A.7)}$$

where b is the radius of the contact area. As indicated in Figure A.1, for a conical indenter with an apex semi-angle of 60°, P_m is related to Y by:

$$P_m = 3.6Y \qquad \textbf{(A.8)}$$

Again, by the use of Tresca's flow criteria, equation A.5 becomes:

$$\sigma_r = \frac{P_i}{3.6} - P_i = -0.7222P_i \qquad \textbf{(A.9)}$$

and equation A.6 is now:

$$\sigma_r = -0.7222H_f \qquad \textbf{(A.10)}$$

for the conical indenter.

APPENDIX B - DERIVATION OF PROJECTED AND CONTACT AREAS

A. VICKER'S INDENTER

As a Vicker's indenter is moved across the sample with a leading plane orientation, three sides are in contact with the sample.

The projected area of the leading plane (Figure B.1(a)) is derived as follows. The triangular area of Figure B.1(b) represents one half of the projected area of the leading plane. This area is:

$$\text{area} = (\tfrac{1}{2})(\text{base})(\text{height}) = (\tfrac{1}{2})c'\ d \qquad \textbf{(B.1)}$$

But:

$$\frac{c'}{d} = \tan(\theta/2) \quad \Rightarrow \quad d = \frac{c'}{\tan(\theta/2)} \qquad \textbf{(B.2)}$$

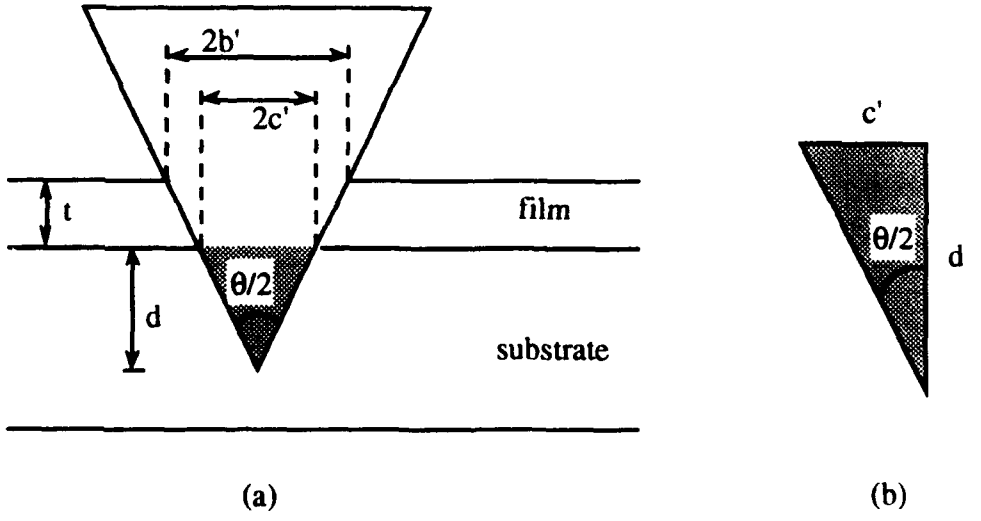

Figure B.1: Projected Area of Contact of Leading Plane: (a) Front View; (b) Geometry of Projected Area.

Substituting equation B.2 into equation B.1 produces:

$$\text{area} = (\tfrac{1}{2})c'^{2}\cot(\tfrac{\theta}{2}) \qquad \textbf{(B.3)}$$

Since this area is only half of the projected area, equation is multiplied by 2:

$$A = c'^{2}\cot(\tfrac{\theta}{2}) \qquad \textbf{(B.4)}$$

where A is the projected area of the leading plane in contact with the substrate. This relationship is used in equation 2.23.

The actual area of contact of the two side planes is derived as follows. Refer to Figure B.2.

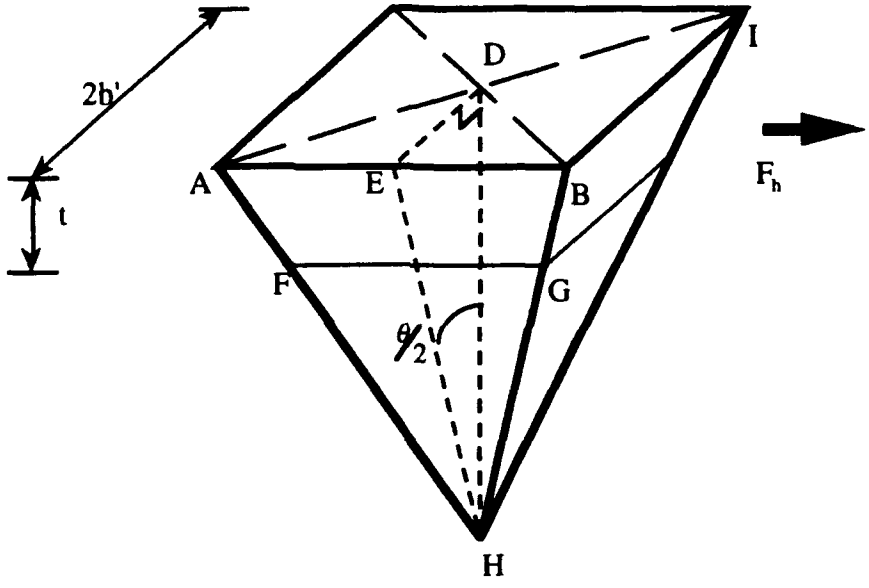

Figure B.2: Actual Area of Contact on the Side Planes for a Leading Plane Orientation.

The base of the indenter is a square, θ/2 is known (68°), t is the film thickness, and length AB (which is the same as BI) is 2b' (measured after the scratch test). The length of face EH is:

$$\overline{EH} = \frac{\overline{DE}}{\sin(\tfrac{\theta}{2})} = \frac{b'}{\sin(\tfrac{\theta}{2})} \qquad \textbf{(B.5)}$$

Therefore, the area of side face ABHA is:

$$\text{ABHA} = 2\left(\tfrac{1}{2}\,\overline{AE}\;\overline{EH}\right) = b'\;\overline{EH} = \frac{b'^2}{\sin(\theta/2)} \qquad \textbf{(P.6)}$$

If area FGHF represents one face in contact with the substrate, then two faces in contact, A_s, is given as:

$$A_s = \frac{2c'^2}{\sin(\theta/2)} \qquad \textbf{(B.7)}$$

where c'=b'- t tan(θ/2). Likewise, area ABFGA represents one face in contact with the film. Two faces in contact, A_f, is given as:

$$A_f = 2\,(\text{ABHA} - \text{FGHF}) = 2\left[\frac{b'^2}{\sin(\theta/2)} - \frac{c'^2}{\sin(\theta/2)}\right] = \frac{2\left(b'^2 - c'^2\right)}{\sin(\theta/2)} \qquad \textbf{(B.8)}$$

The results in equations B.7 and B.8 are used in equations 2.24 and 2.25.

B. CONICAL INDENTER

The force required to overcome the shear between the film or substrate and the indenter can be determined by considering the incremental force dF acting over an incremental area dA. Referring to Figure B.3(a), dA may be derived as follows [Ref.26]:

$$dA = r\,d\gamma\,dS \qquad \textbf{(B.9)}$$

As shown in Figure B.3(b):

$$\frac{dr}{dS} = \sin(\theta/2) \quad \Rightarrow \quad dS = \frac{dr}{\sin(\theta/2)} \qquad \textbf{(B.10)}$$

Substituting equation B.10 into equation B.9 produces:

$$dA = \frac{r\,dr\,d\gamma}{\sin(\theta/2)} \qquad \textbf{(B.11)}$$

Equation B.11 is used as equation 2.44.

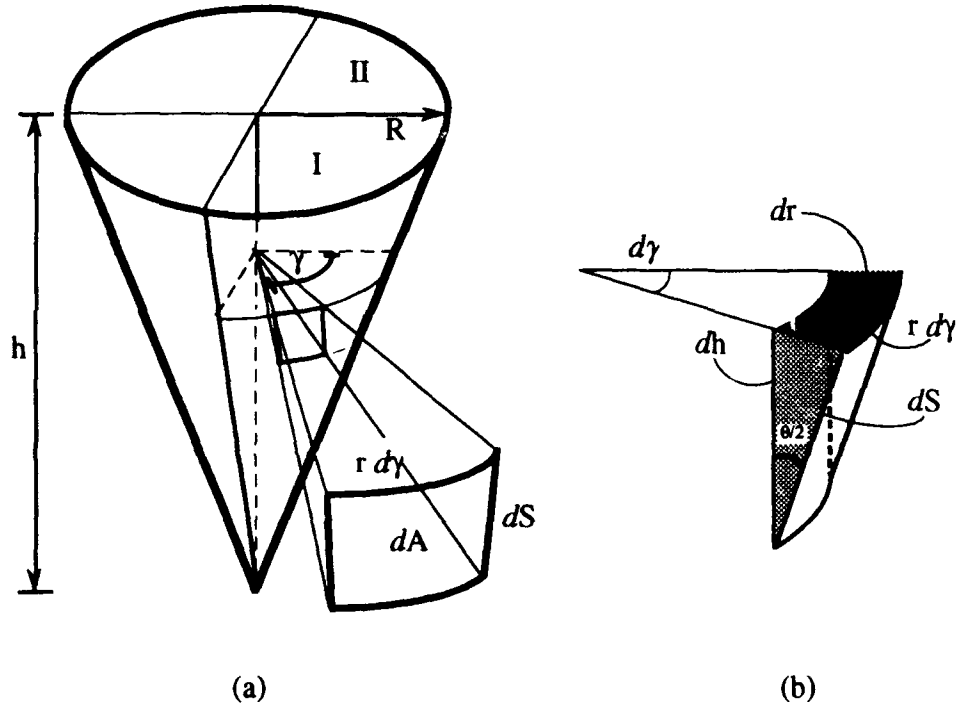

(a) (b)

Figure B.3: Derivation of *d*A: (a) Position of *d*A on Conical Indenter; (b) Relationship of *d*A to r and γ.

APPENDIX C - DERIVATION OF AREA OF FILM REMOVAL DURING FORWARD LATERAL FLAKING

The area of film removed in front of the indenter due to the forward lateral flaking (FLF) mode of failure can be approximated by a circle. A portion of this circle is not considered due to the protrusion of the indenter (see Figure C.1). Area A_{BCDB} is the area of interest.

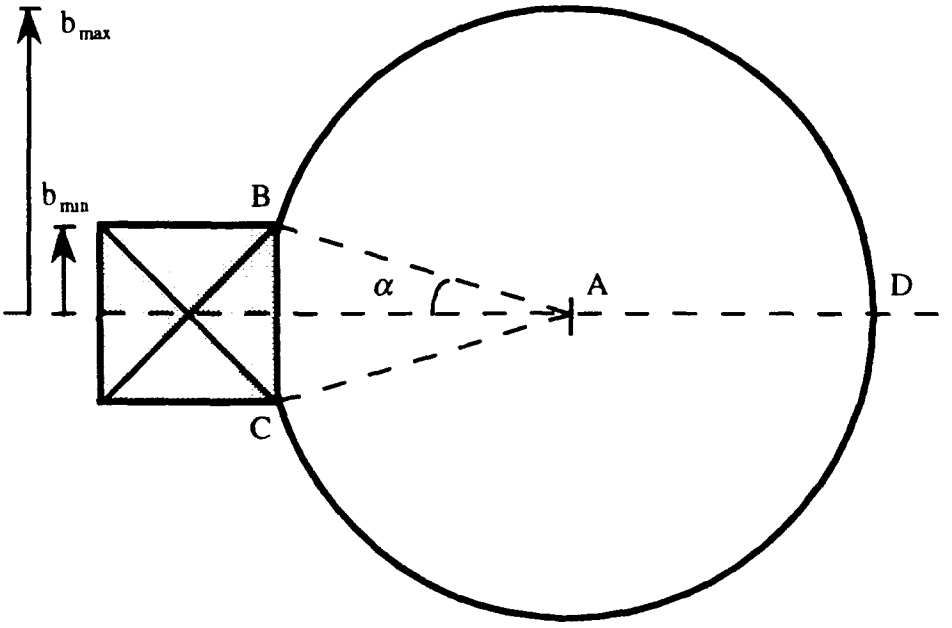

Figure C.1: Geometry of Material Removed during FLF.

$$A_{BCDB} = A_{circle} - A_{section\ ABCA} + A_{\Delta\ ABCA} \qquad \textbf{(C.1)}$$

where

$$A_{circle} = \pi\ b_{max}^2$$

$$A_{arc\ ABC} = \left(\frac{2\alpha}{2\pi}\right)\pi\ b_{max}^2 = \alpha\ b_{max}^2$$

$$A_{\Delta\ ABC} = (b_{min})(b_{max}\cos\alpha)$$

Equation C.1 becomes:

$$A_{BCDB} = \pi\ b_{max}^2 - \alpha\ b_{max}^2 + (b_{min})(b_{max}\cos\alpha) \qquad \textbf{(C.2)}$$

where

$$\alpha = \sin^{-1}\left(b_{min}/b_{max}\right)$$

Substituting α into equation C.2 produces:

$$A_{BCDB} = \pi\ b_{max}^2 - b_{max}^2\sin^{-1}\left(b_{min}/b_{max}\right) + b_{min}b_{max}\cos\left[\sin^{-1}\left(b_{min}/b_{max}\right)\right] \qquad \textbf{(C.3)}$$

Equation C.3 is defined as A_{FLF}, and is used as equation 3.2.

APPENDIX D - IBM-BASIC DATA COLLECTION ALGORITHM AND PROGRAM

This program controls the data acquisition (DAQ) system, collects the instrumentation voltage outputs, and then converts and stores the resultant data.

1. Interface Hewlett-Packard 3852A DAQ/Control Unit with IBM personal computer.
2. Enter initial zero load (offset) parameters.
   a. LVDT
   b. horizontal load cell
   c. vertical load cell
3. Verify inputs are correct.
4. Dimensionalize arrays.
5. Enter data collection run parameters.
   a. number of channels
   b. number of scans
6. Record instrumentation output voltages.
   a. channel 205: LVDT
   b. channel 206: horizontal load cell
   c. channel 207: 10 VDC power supply (monitoring only)
   d. channel 208: vertical load cell
7. Auto-end program if either load cell is overranged; allow for input errors from DAQ system.
8. Subtract initial offset values; display raw data.
9. Bypass data conversion if run was for only obtaining initial offset values.

10. Save raw data if desired (RAW##.DAT).
11. Convert raw data to appropriate units.
    a. LVDT: centimeters (cm)
    b. horizontal load cell: newtons (N)
    c. 10 VDC power supply: leave as DC volts (VDC)
    d. vertical load cell: newtons (N)
12. Display results.
    a. column 1: distance (cm)
    b. column 2: horizontal force (N)
    c. column 3: 10 VDC power supply (VDC)
    d. column 4: vertical force (N)
13. Save result data if desired (RESULT##.DAT).
14. Prompt user for another run.

```
**************************************************************************************
1000    '*************************************************************************
1010  '
1020  '              PROGRAM COLLECT.BAS
1030  '
1040  '               REVISION DATE 931027
1050    '*************************************************************************
1060  'THIS PROGRAM IS USED DURING A SCRATCH TEST TO COLLECT DATA TO BE USED TO
1070  'DETERMINE THE INTERFACIAL SHEAR STRENGTH AT THIN FILM-CERAMIC BOUNDARIES
1080  'IN REAL TIME. PRIMARY ROUTINES FOR METRABYTE IEEE-488 BOARD TO HP-3852
1090  'DATA ACQUISITION UNIT (WRITTEN BY TOM CHRISTIAN) USE 44702A HIGH SPEED
1100  'VOLTMETER AND 447711A FET MUX CARD. PORTIONS OF THIS PROGRAM WERE
1110  'WRITTEN BY DAVE LASCURAIN AND DAN SECOR.
1120    '*************************************************************************
1130 PRINT "ENSURE ONLY THE VOLTMETER IS ON BEFORE TESTING"
1140 CLEAR
```

```
1150 DEF SEG = &HD000
1160 GPIB = 0: FLG% = 0: BRD% = 0: DUMMY% = 0'CLEAR VARIABLES
1170  '
1180      '*************************************************************************
1190  'SETUP METRABYTE INTERFACE BOARD
1200 INIT$ = "SYSCON MAD=3,CIC=1,NOB=1,BA0=&H300"
1210  'SYSCON    IS SET UP COMMAND TO INITIALIZE AND CONFIGURE BOARD
1220  'MAD       IS MY ADDRESS EQUALS THREE
1230  'CIC       IS CONTROLLER IN CHARGE EQUALS ONE
1240  'NOB       IS NUMBER OF BOARDS EQUALS ONE
1250  'BA0       IS BASE I/O ADDRESS OF BOARD
1260 CONF$ = "CONFIG MTA,LISTEN=9"   'PREPARE DEVICE 9 AS LISTENER
1270 REMOT$ = "REMOTE 9"           'PLACE DEVICE 9 IN REMOTE MODE
1280 CMDOUT$ = "OUTPUT 9[$E]       'BEGINING OF OUTPUT STRING"
1290 CMDIN$ = "ENTER 9[$,0,18]     'INPUT STRING FOR 19 CHARCTERS"
1300 CLR$ = "CLEAR 9"              'CLEAR DEVICE 9
1310 DAT$ = SPACE$(20)             'DIMENSION MEMORY FOR DATA
1320  '
1330      '*************************************************************************
1340  'PREPARE METRABYTE INTERFACE BOARD
1350  'CALL INTERPRETER IN ROM TO ACCESS BOARD AND RETURN FLAG INFO
1360 CMD$ = INIT$
1370 GOSUB 3280
1380 CMD$ = CONF$
1390 GOSUB 3280
1400 CMD$ = CLR$
1410 GOSUB 3280
1420 CMD$ = REMOT$
1430 GOSUB 3280
1440  '
1450      '*************************************************************************
1460  'SETUP 3852 VOLTMETER ETC
1470 MSG$ = "RESET 000"            'RESET VOLTMETER IN SLOT 0
1480 GOSUB 3310
```

```
1490 MSG$ = "USE 000"            'USE VOLTMETER FOR MEASURMENTS
1500 GOSUB 3310
1510 MSG$ = "CONF DCV"           'CONFIGURE FOR DC VOLTS
1520 GOSUB 3310
1530 '
1540     '*************************************************************************
1550 'DETERMINE INITIAL OFFSET VALUES. INITIAL OFF SET VALUES ON INSTRUMENTS
1560 'WITHOUT ANY LOADS APPLIED ARE SUBTRACTED FROM TRUE LOAD READINGS
1570 'MEASURED DURING THE SCRATCH TEST.
1580 PRINT " "
1590 PRINT "IS THIS RUN ONLY FOR OBTAINING THE INITIAL VALUES OF"
1600 INPUT "LOAD CELLS AND LVDT? (Y/N) ", VALU$
1610 PRINT " "
1620 PRINT "INITIAL VOLTAGE OF TABLE LVDT MIGHT BE NEGATIVE. ENSURE"
1630 PRINT "YOU KNOW WHETHER YOU ARE ON THE + OR - SIDE OF THE NULL FOR"
1640 PRINT "THE INITIAL LVDT VOLTAGE!"
1650 PRINT " "
1660 INPUT "ENTER INITIAL VOLTAGE OF TABLE LVDT (volts) ", VCM
1670 PRINT "HORIZONTAL LOAD CELL INITIAL VOLTAGE INCLUDES THAT FORCE TO MOVE";
1680 PRINT " TABLE "
1690 INPUT "ENTER INITIAL VOLTAGE OF HORIZONTAL LOAD CELL (volts) ", VHORZ
1700 INPUT "ENTER INITIAL VOLTAGE OF VERTICAL LOAD CELL (volts) ", VVERT
1710 PRINT " "
1720 PRINT "INITIAL VOLTAGE OF TABLE LVDT (volts) = ", VCM
1730 PRINT "INITIAL VOLTAGE OF HORIZONTAL LOAD CELL (volts) = ", VHORZ
1740 PRINT "INITIAL VOLTAGE OF VERTICAL LOAD CELL (volts) = ", VVERT
1750 PRINT " "
1760 INPUT "DO YOU AGREE WITH THESE VALUES IN VOLTS? (Y/N) ", QUES$
1770 IF QUES$ = "n" OR QUES$ = "N" GOTO 1660
1780 INPUT "HOW MANY CHANNELS DO YOU WISH TO USE (MAX IS 4) ", ADSTOP
1790 ADSTOP = ADSTOP - 1
1800 IF ADSTOP > 4 THEN GOTO 1780
1810 PRINT "PROGRAM RUNS AUTOMATICALLY AFTER THE NEXT INPUT. START TABLE, AND"
1820 PRINT "COMMENCE PROGRAM AS TABLE PASSES THROUGH ZERO REFERENCE POSITION."
```

```
1830 INPUT "HOW MANY TIMES DO YOU WISH TO SAMPLE THESE CHANNELS ", SCANS
1840 PRINT "WARNING IF SCREEN SAVER COMES ON PROGRAM STOPS TAKING DATA!!"
1850 '
1860 '*****************************************************************************
1870 'SETUP ARRAYS FOR DATA STORAGE
1880 DIM VOLTS(SCANS, ADSTOP) 'PREPARE AN ARRAY FOR RAW DATA
1890 DIM RESULTS(SCANS, ADSTOP) 'PREPARE AN ARRAY FOR RESULTS
1900 DIM W(SCANS)      'PREPARE AN ARRAY FOR VERTICAL LOAD (NEWTONS)
1910 DIM FH(SCANS)     'PREPARE AN ARRAY FOR HORIZONTAL LOAD (NEWTONS)
1920 DIM CM(SCANS)     'PREPARE AN ARRAY FOR DISTANCE (CM)
1930 DIM VDC(SCANS)    'PREPARE AN ARRAY FOR POWER SUPPLY TO HORZ LOAD CELL
1940 '
1950 '*****************************************************************************
1960 'BEGIN TO TAKE RAW DATA
1970 STRTIM = TIMER            'GET START TIME
1980 ALARM = 0                 'RESET FALSE ALARM COUNT TO ZERO
1990 FOR NO = 1 TO SCANS       'USE NESTED LOOPS FOR SCANS AND CHANNELS
2000 FOR CH = 0 TO ADSTOP      'USE FOR/NEXT LOOP AS CHANNELS
2010 J = 205 + CH              'CHANNELS = 205 PLUS CH
2020 CHNL$ = STR$(J)           'COMMAND TO 3852 MUST BE IN STRINGS
2030 MSG$ = "MEAS DCV," + CHNL$   'MEASURE VOLTAGE ON CHANNEL 205 PLUS CH
2040 GOSUB 3310
2050 GOSUB 3340                'CALL ENTER ROUTINE
2060 VOLTS(NO, CH) = VAL(DAT$)    'DATA IS RETURNED IN DAT$
2070 'AND CONVERTED TO REAL NUMBER
2080 'THE NEXT 18 LINES DETERMINE IF THE HORIZONTAL OR VERTICAL LOAD CELL
2090 'HAS BEEN EXCEEDED. IF SO, AN ALARM SOUNDS. A COMPUTER GLITCH MAY CAUSE
2100 'A FALSE ALARM, BUT IF THIS HAPPENS THREE TIMES, THE PROGRAM IS ENDED.
2110 IF CH = 0 OR CH = 2 GOTO 2260
2120 IF CH = 1 THEN GOTO 2140
2130 IF CH = 3 THEN GOTO 2170
2140 IF VOLTS(NO, CH) < (.0117 + VHORZ) THEN GOTO 2260
2150 PRINT "HORIZONTAL FORCE EXCEEDED 400 GRAMS!!!!!"
2160 GOTO 2190
```

```
2170 IF VOLTS(NO, CH) < (.3509) THEN GOTO 2260
2180 PRINT "VERTICAL FORCE + PRE-LOAD EXCEEDED 1500 GRAMS!!!!!"
2190 FOR CNT = 1 TO 12
2200 BEEP
2210 NEXT CNT
2220 ALARM = ALARM + 1
2230 IF ALARM < 3 THEN GOTO 2260
2240 PRINT "LOAD CELL RANGE EXCEEDED; PROGRAM ENDED"
2250 END
2260 NEXT CH
2270 NEXT NO
2280 STPTIM = TIMER              'GET STOP TIME
2290 TOTIME = STPTIM - STRTIM    'CALCULATE ELAPSED TIME
2300 MSG$ = "BEEP"               'MAKE 3852 BEEP WHEN DONE
2310 GOSUB 3310
2320 CMD$ = CLR$                 'CLEAR AND RESET DEVICE 9
2330 GOSUB 3280
2340 '
2350 '*****************************************************************************
2360 'PRINT RAW DATA. THE MEASURED VALUE DURING THE SCRATCH TEST HAS THE
2370 'INITIAL OFFSET VALUE SUBTRACTED OFF IN THE STEPS BELOW.
2380 PRINT " "
2390 PRINT "  DIST (vdc)  FH (vdc)  PWR (vdc)   W (vdc)"
2400 FOR NO = 1 TO SCANS
2410 FOR CH = 0 TO ADSTOP
2420 IF CH = 0 THEN VOLTS(NO, CH) = ABS(VOLTS(NO, CH) - VCM)
2430 CM0 = VOLTS(1, 0)
2440 IF CH = 0 THEN VOLTS(NO, CH) = VOLTS(NO, CH) - CM0
2450 'THESE LAST TWO LINES SET THE POSITION OF THE FIRST DATA POINT AT
2460 'ZERO. ALL OTHER POINTS ARE NOW WRT THE FIRST DATA POINT.
2470 IF CH = 1 THEN VOLTS(NO, CH) = VOLTS(NO, CH) - VHORZ
2480 IF CH = 3 THEN VOLTS(NO, CH) = VOLTS(NO, CH) - VVERT
2490 PRINT USING "####.######"; VOLTS(NO, CH);
2500 PRINT CHR$(32);
```

```
2510 NEXT CH
2520 PRINT " "
2530 NEXT NO
2540 PRINT " "
2550 IF VALU$ = "Y" OR VALU$ = "y" GOTO 3250  'BYPASSES SHEAR CALCULATIONS IF
2560  'ONLY INITIAL VALUES ARE DESIRED.
2570 PRINT "TOTAL ELAPSED FOR DATA ACQUISITION = ";
2580 PRINT USING "###.##"; TOTIME;
2590 PRINT "   SECONDS"
2600 PRINT "THE INITIAL OFFSETS HAVE BEEN SUBTRACTED FROM EACH"
2610 PRINT "RESPECTIVE OUTPUT"
2620 PRINT " "
2630 INPUT "DO YOU WISH TO SAVE THE RAW DATA  (Y/N)  ", QUES$
2640 IF QUES$ = "N" OR QUES$ = "n" GOTO 2780
2650 INPUT "ENTER THE NAME OF THE DATA FILE TO CREATE (IE RAW##.DAT)  ", FILE$
2660 OPEN FILE$ FOR OUTPUT AS 1
2670 FOR NO = 1 TO SCANS
2680 FOR CH = 0 TO ADSTOP
2690 PRINT #1, USING "####.######"; VOLTS(NO, CH);  'REMEMBER THAT OFFSET
2700  'VALUES WERE SUBTRACTED
2710 PRINT #1, CHR$(9);
2720 NEXT CH
2730 PRINT #1, " "
2740 NEXT NO
2750 CLOSE #1
2760  '
2770     '*************************************************************************
2780  'CONVERSION OF RAW DATA
2790 FOR NO = 1 TO SCANS
2800 FOR CH = 0 TO ADSTOP
2810 IF CH = 0 THEN CM(NO) = .122988885# * VOLTS(NO, CH)
2820  'CONVERTS VOLTS TO CENTIMETERS
2830 IF CH = 1 THEN FH(NO) = 34246.57534# * VOLTS(NO, CH) * .00981
2840  'CONVERTS VOLTS TO GRAM FORCE HORZ AND THEN TO NEWTONS
```

```
2850 IF CH = 2 THEN VDC(NO) = VOLTS(NO, CH)
2860  'DISPLAYS 10vdc POWER SUPPLY OUTPUT
2870 IF CH = 3 THEN W(NO) = 6732.4942# * VOLTS(NO, CH) * .00981
2880  'CONVERTS VOLTS TO GRAM FORCE VERT AND THEN TO NEWTONS
2890 NEXT CH
2900 NEXT NO
2910  '
2920      '*************************************************************************
2930  'PRINT RESULTS DATA
2940 PRINT " "
2950 PRINT "   DIST (cm)   FH (N)     PWR (vdc)   W(N)"
2960 FOR NO = 1 TO SCANS
2970 PRINT USING "####.######"; CM(NO); FH(NO); VDC(NO); W(NO);
2980 PRINT " "
2990 NEXT NO
3000 PRINT " "
3010 PRINT "!!ENSURE THE FOLLOWING DATA IS RECORDED!!"
3020 PRINT "TOTAL ELAPSED TIME (sec) FOR DATA ACQUISITION = ", TOTIME
3030 PRINT " "
3040 PRINT " "
3050  '
3060      '*************************************************************************
3070  'GENERATE RESULT DATA FILE
3080 INPUT "DO YOU WISH TO SAVE THE RESULTS DATA  (Y/N)  ", QUES$
3090 IF QUES$ = "N" OR QUES$ = "n" GOTO 3250
3100 INPUT "ENTER NAME OF THE DATA FILE TO CREATE (IE RESULT##.DAT)  ", FILE$
3110 OPEN FILE$ FOR OUTPUT AS 1
3120 FOR NO = 1 TO SCANS
3130 PRINT #1, USING "####.######"; CM(NO);
3140 PRINT #1, CHR$(9);
3150 PRINT #1, USING "####.######"; FH(NO);
3160 PRINT #1, CHR$(9);
3170 PRINT #1, USING "####.######"; VDC(NO);
3180 PRINT #1, CHR$(9);
```

```
3190 PRINT #1, USING "####.######"; W(NO);
3200 PRINT #1, " "
3210 NEXT NO
3220 CLOSE #1
3230  '
3240      '*************************************************************************
3250 INPUT "WOULD YOU LIKE TO TRY ANOTHER RUN (Y/N) ", QUES2$
3260 IF QUES2$ = "Y" OR QUES2$ = "y" GOTO 1140
3270 END
3280 CALL GPIB(CMD$, DUMMY%, FLG%, BRD%)
3290 IF FLG% <> 0 THEN PRINT " ERROR IN "; CMD$; VAR$; "FLAG = HEX "; HEX$(FLG%)
3300 RETURN
3310 CALL GPIB(CMDOUT$, MSG$, FLG%, BRD%)
3320 IF FLG% <> 0 THEN PRINT " ERROR IN "; MSG$; "FLAG = HEX "; HEX$(FLG%)
3330 RETURN
3340 CALL GPIB(CMDIN$, DAT$, FLG%, BRD%)
3350 IF FLG% <> 0 THEN PRINT " DATA INPUT ERROR FLAG = HEX "; HEX$(FLG%)
3360 RETURN
*****************************************************************************************
```

APPENDIX E - IBM-BASIC DATA EVALUATION ALGORITHM AND PROGRAM

This program retrieves the result data file generated by the program of Appendix D. It then evaluates the data based on user inputs to calculate the interfacial shear strength.

1. Dimensionalize arrays.
2. Enter result data file to be evaluated (RESULT##.DAT).
3. Enter baseline data.
   a. use one base data file or use average of two base data files
   b. enter corrections VOFF and HOFF to RESULT data file so that RESULT data and BASE data zero references are coincident
4. Subtract baseline data from RESULT data to obtain net horizontal force.
5. Enter data for shear stress calculations.
   a. half track max width, BMAX
   b. half track min width, BMIN
   c. film thickness, T
   d. Poisson's ration of film, NU
   e. Vicker's hardness of substrate, VHN
6. Unit conversion of input data.
   a. BMAX, BMIN, T: meters (m)
   b. VHN: indentation hardness (N/m^2)
7. Calculate various constants and parameters required for shear values.
   a. half track width of indenter/substrate interface, C (equation 2.30)
   b. constant for Bessel function, PHI (equation 2.30)
   c. argument for Bessel function, Z (equation 2.30)

d. circular area of flake removal, AREA (equation 3.2)

8. Calculate shear values for each scan.
   a. film indentation hardness, HFILM (equation 2.21)
   b. perform double integral to calculate average shear stress due to vertical load only, TIHV (equation 3.14)
   c. average shear stress to debond film due to horizontal load TIEFF (equation 3.4)
9. Display shear data.
   a. column 1: TIHV (MPa)
   b. column 2: TIEFF (MPa)
   c. column 3: TI (MPa) (equation 3.15)
10. Save shear data if desired.
11. Prompt user for another evaluation of same RESULT data file.

```
1000    '*************************************************************************
1010  '
1020  '                          PROGRAM EVALUAT.BAS
1030  '
1040  '                                        *  *  *
1050  '                      VICKER'S INDENTER   *     * --->
1060  '                                        *  *  *
1070  '
1080  '                          REVISION DATE  931205
1090    '*************************************************************************
1100  'THIS VERSION OF EVALUAT0.BAS (original) HAS BEEN MODIFIED TO ACCOUNT FOR
1110  'FLAKING OF THE FILM IN FRONT OF THE INDENTER.  BASELINE DATA IS USED.
1120  'TYPE III SHEAR IS INTEGRATED OVER THE AREA IN FRONT OF THE INDENTER.
1130  'THE PROGRAM ENABLES THE USER TO EVALUATE THE RITTER SHEAR STRESS (TIHV)
1140  'AND THE BENJAMIN SHEAR STRESS (TIEFF) BASED ON USER INPUTS.
```

```
1150 '
1160 '*************************************************************************
1170 'DIMENSIONALIZE ARRAYS
1180 DIM W(325)              'ARRAY FOR VERTICAL LOAD
1190 DIM FH(325)             'ARRAY FOR HORIZONTAL LOAD
1200 DIM HOR(325)            'ARRAY FOR MODIFIED HORIZONTAL LOAD
1210 DIM BASE(325)           'ARRAY FOR BASELINE
1220 DIM SHEAR(325, 3)       'ARRAY FOR DATA PRINTING; CHANGE 3 BACK TO 4 WHEN
1230                         'USING DISTANCE COLUMN
1240 DIM TIHV(325)           'ARRAY FOR RITTER SHEAR STRESS
1250 DIM TIEFF(325)          'ARRAY FOR BENJAMIN SHEAR STRESS
1260 DIM FINAL$(325, 3)      'ARRAY FOR DATA OUTPUT
1270 DIM FILE$(325, 4)       'ARRAY FOR DATA INPUT
1280 DIM A(325, 4)           'ARRAY FOR HOLDING FIRST BASELINE DATA
1290 DIM B(325, 4)           'ARRAY FOR HOLDING SECOND BASELINE DATA
1300 DIM C(325, 4)           'ARRAY FOR HOLDING RESULT DATA
1310 DIM L(102)              'ARRAY FOR LAMDA VALUES FOR INTEGRATION
1320 DIM R(102)              'ARRAY FOR RADIUS VALUES FOR INTEGRATION
1330 DIM F(102)              'ARRAY FOR INTERMEDIATE INTEGRATION
1340 DIM T(102)
1350 '
1360 '*************************************************************************
1370 'INPUT RESULT FILE TO BE ANALYZED
1380 INPUT "ENTER THE DATE OF THIS EVALUATION (YYMMDD). ", DATE
1390 INPUT "WHICH RESULT##.DAT IS TO BE EVALUATED? ", FILE$
1400 INPUT "HOW MANY DATA SETS ARE IN THE RESULT FILE? ", SCANS
1410 OPEN FILE$ FOR INPUT AS 3
1420 FOR NO = 1 TO SCANS
1430 FOR CH = 0 TO 3
1440 INPUT #3, C(NO, CH)
1450 IF CH = 1 THEN FH(NO) = C(NO, CH)
1460 IF CH = 3 THEN W(NO) = C(NO, CH)
1470 NEXT CH
1480 NEXT NO
```

```
1490 CLOSE #3
1500 PRINT " "
1510 '
1520 '*************************************************************************
1530 'INPUT BASELINE DATA. EITHER USE ONE BASELINE DATA FILE, OR USE THE
1540 'AVERAGE OF TWO BASELINE DATA FILES.
1550 PRINT "DO YOU DESIRE TO SUBRACT ONE BASELINE OR THE AVERAGE OF TWO"
1560 INPUT "BASELINES FROM RESULTS FILE? ENTER EITHER (1) OR (2). ", CHOICE
1570 IF CHOICE = 2 THEN GOTO 1680
1580 INPUT "ENTER THE BASELINE FILE TO BE USED. (BASE##AorB.DAT) ", FILE$
1590 OPEN FILE$ FOR INPUT AS 1
1600 FOR NO = 1 TO SCANS
1610 FOR CH = 0 TO 3
1620 INPUT #1, A(NO, CH)
1630 IF CH = 1 THEN BASE(NO) = A(NO,CH)
1640 NEXT CH
1650 NEXT NO
1660 CLOSE #1
1670 GOTO 1810
1680 INPUT "ENTER THE FIRST BASELINE FILE TO BE USED. (BASE##A.DAT) ", FILE$
1690 OPEN FILE$ FOR INPUT AS 1
1700 INPUT "ENTER THE SECOND BASELINE FILE TO BE USED. (BASE##B.DAT) ", FILE$
1710 OPEN FILE$ FOR INPUT AS 2
1720 FOR NO = 1 TO SCANS
1730 FOR CH = 0 TO 3
1740 INPUT #1, A(NO, CH)
1750 INPUT #2, B(NO, CH)
1760 IF CH = 1 THEN BASE(NO) = (A(NO,CH) + B(NO,CH)) / 2
1770 NEXT CH
1780 NEXT NO
1790 CLOSE #1
1800 CLOSE #2
1810 PRINT " "
1820 '
```

```
1830    '*************************************************************************
1840  'ENSURE BOTH RESULT DATA FILE AND BASE DATA FILE HAVE THE SAME ZERO
1850  'START POINT.
1860 PRINT "ENTER THE VERTICAL SHIFT FOR THE HORIZONTAL"
1870 INPUT "FORCE REFERENCE POINT.  ", VOFF
1880 PRINT " "
1890 PRINT "ENTER THE HORIZONTAL SHIFT FOR THE HORIZONTAL REFERENCE POINT."
1900 INPUT "SLIDING THE FH COLUMN UP (DOWN) REQUIRES A + (-) NUMBER.  ", HOFF
1910  '
1920    '*************************************************************************
1930  'CALCULATE THE NET HORIZONTAL FORCE VALUES
1940 FOR NO = 1 TO SCANS
1950 HOR(NO) = FH(ABS(NO+HOFF)) + VOFF - BASE(NO)  'IF FH COLUMN HAD TO BE SLID
1960  'DOWN, YOU WOULD HAVE FH(-#).  ABS CHANGES THIS TO A +#.  SINCE THE
1970  'FIRST SEVERAL DATA POINTS ARE FROM THE NO-LOAD PORTION OF THE RUN, THIS
1980  'DOES NOT AFFECT THE RESULTS.
1990 NEXT NO
2000 PRINT " "
2010 PRINT " "
2020  '
2030    '*************************************************************************
2040  'INPUT THE SCRATCH TRACK DATA AND MATERIAL PROPERTIES
2050 INPUT "ENTER BMAX, THE HALF TRACK MAX WIDTH (um)  ", BMAX
2060 INPUT "ENTER BMIN, THE HALF TRACK MIN WIDTH (um)  ", BMIN
2070 INPUT "ENTER T, THE FILM THICKNESS (um) (0.4)  ", T
2080 INPUT "ENTER NU, THE POISSONS RATIO OF FILM (Cr BULK = 0.21)  ", NU
2090  PI  =  3.14159265359#
2100 THETA = (136 / 180 * PI)      'CONVERTS VICKERS ANGLE TO RADIANS
2110 C = BMIN - (T * TAN(THETA / 2)) 'HALF TRACK WIDTH OF
2120  'INDENTER/SUBSTRATE INTERFACE
2130 PRINT "    VICKERS HARDNESS NUMBER, VHN = 557.7 Kg/mm^2 FOR GLASS"
2140 PRINT "    BASED ON RITTER HAND CALCULATION DATA"
2150 INPUT "ENTER VHN, THE SUBSTRATE VICKERS HARDNESS NUMBER (Kg/mm^2)  ", VHN
2160 HS = 1.0785 * VHN    'CONVERTS VHN TO INDENTATION HARDNESS (Kg/mm^2)
```

```
2170 HS = HS * 9.81E6    'CONVERTS INDENTATION HARDNESS (Kg/mm^2) TO (N/m^2)
2180 FOR CNT = 1 TO 10
2190 PRINT " "
2200 NEXT CNT
2210 PRINT "DATE OF EVALUATION IS ", DATE
2220 PRINT "INDENTATION HARDNESS OF SUBSTRATE (N/m^2) HS= ", HS
2230 PRINT "THE HALF TRACK MAX WIDTH (um) BMAX= ", BMAX
2240 PRINT "THE HALF TRACK MIN WIDTH (um) BMIN= ", BMIN
2250 PRINT "THE HALF TRACK WIDTH OF INDENTER/SUBSTRATE INTERFACE (um) C= ", C
2260 RATIO1 = BMIN / BMAX   'USED FOR CACULATING INV SIN
2270 PRINT "FILM THICKNESS (um) T= ", T
2280 BMAX = BMAX / 1E6   'CONVERTS HALF TRACK MAX WIDTH (um) TO (m)
2290 BMIN = BMIN / 1E6   'CONVERTS HALF TRACK MIN WIDTH (um) TO (m)
2300 C = C / 1E6    'CONVERTS C (um) TO (m)
2310 T = T / 1E6   'CONVERTS FILM THICKNESS (um) TO (m)
2320 PRINT "POISSONS RATIO OF FILM  NU=  ", NU
2330  '
2340      '*************************************************************************
2350  'DETERMINE VARIOUS CONSTANTS AND PARAMETERS REQUIRED FOR SHEAR VALUES.
2360 ALFA = ATN(RATIO1 / SQR(-RATIO1 * RATIO1 + 1))  'THIS IS THE COMPUTER'S
2370  'WAY OF CALCULATING INV SIN(RATIO).  ALFA IS THE ANGLE BETWEEN THE
2380  'HORIZONTAL AND THE LINE BETWEEN THE CENTER OF THE FLAKE CIRCLE AND THE
2390  'CORNER OF THE INDENTER.
2400 PHI = SQR(6 * (1 - NU) / (4 + NU))     'USED IN BESSEL FUNC APPROX
2410 AREA = BMAX ^ 2 * (PI - ALFA) + BMAX * BMIN * COS(ALFA)  'THIS IS THE
2420  'AREA (m^2) IN FRONT OF THE INDENTER OVER WHICH THE SHEAR STRESSES ACT.
2430 PRINT "AREA OF FLAKING IN FRONT OF THE INDENTER (m^2) =  ", AREA
2440 Z = SQR(2) * PHI * BMIN / T       'ARGUMENT FOR BESSEL FUNC
2450 PRINT "PHI = ", PHI, " ", "Z = ", Z
2460 FOR NO = 1 TO SCANS
2470 HFILM = (W(NO) - 3 * HS * C ^ 2) / (3 * (BMIN ^ 2 - C ^ 2))   '(N/m^2)
2480  'FIND FILM HARDNESS FROM APPLYING HOWES & RYAN MATH
2490  '
2500      '*************************************************************************
```

```
2510 'DOUBLE INTEGRATION OF THE TYPE III SHEAR OVER THE AREA OF FLAKE CIRCLE.
2520 M = BMIN + BMAX * COS(ALFA)  'DISTANCE FROM CENTER OF INDENTER TO CENTER
2530  'OF FLAKE CIRCLE
2540 E = (M ^ 2 - BMAX ^ 2)      'COMBINING TWO CONSTANTS FOR FUTURE USE
2550 N = 8                       'NUMBER OF INTERVALS FOR SIMPSONS RULE
2560 RATIO2 = BMAX / M           'USED FOR CALCULATING INV SIN
2570 LOWLAM = 0                  'LOWER LIMIT OF INTEGRATION WRT LAMDA.
2580  'LAMDA IS THE ANGLE FORMED BY THE HORIZONTAL AND A LINE FROM THE INDENTER
2590  'CENTER TO A TANGENT OF THE FLAKE CIRCLE.
2600 UPLAM = ATN(RATIO2 / SQR(-RATIO2 * RATIO2 + 1))  'UPPER LIMIT OF
2610  'INTEGRATION WRT LAMDA
2620 LAMINT = (UPLAM - LOWLAM) / N  'LAMDA INTERVAL SIZE
2630 FOR I = 1 TO N + 1
2640 L(I) = LOWLAM + (I - 1) * LAMINT
2650 LOWRAD = SQR(2) * BMIN    'LOWER LIMIT OF INTEGRATION WRT RADIUS
2660 UPRAD = M * COS(L(I)) + SQR(ABS(M ^ 2 * (COS(L(I))) ^ 2 - E))  'UPPER
2670  'LIMIT OF INTEGRATION WRT RADIUS.  AS THE PROGRAM APPROACHES THE UPPER
2680  'LIMIT OF THE VARIABLE R, THE SQR(xxx) APPROACHES ZERO.  HOWEVER, DUE TO
2690  'COMPUTER ACCURACY, xxx MIGHT BE COMPUTED AS A NEGATIVE NUMBER TO THE
2700  'ORDER 10E-18.  THIS IS ESSENTIALLY ZERO, BUT THE COMPUTER ERRORS ON
2710  'TAKING THE SQUARE OF A NEGATIVE NUMBER, HENCE THE ABS VALUE IS USED.
2720 RADINT = (UPRAD - LOWRAD) / N
2730 FOR H = 1 TO N + 1
2740 R(H) = LOWRAD + (H - 1) * RADINT
2750  'THE FOLLOWING FOUR LINES ARE THE ACTUAL EQUATION WHICH IS BEHIND THE
2760  'DOUBLE INTEGRAL. DEN IS THE EQUATION; NUM, DEN1, AND DEN2 JUST BUILD IT.
2770 NUM = 2 * (-.6875) * HFILM * PHI^2 * R(H)^2 * (1 + (3 * T) / (8 * PHI * R(H)) +
        (-15 * T ^ 2) / (128 * PHI ^ 2 * R(H) ^ 2))
2780  'MULTIPLIED BY 2 SINCE THE INTEGRATION WAS OVER ONLY HALF THE AREA
2790 DEN1 = -1 * PHI * R(H) * (1 + (7 * T) / (8 * PHI * R(H)) + (57 * T ^ 2) / (128 * PHI ^ 2 * R(H) ^ 2))
2800 DEN2 = NU * T * (1 + (3 * T) / (8 * PHI * R(H)) + (-15 * T ^ 2) / (128 * PHI ^ 2 * R(H) ^ 2))
2810 DEN = DEN1 + DEN2
2820 T(H) = NUM / DEN
2830 NEXT H
```

```
2840 SUMEVE = 0
2850 FOR H = 2 TO N STEP 2
2860 SUMEVE = SUMEVE + T(H)
2870 NEXT H
2880 SUMODD = 0
2890 FOR H = 3 TO N - 1 STEP 2
2900 SUMODD = SUMODD + T(H)
2910 NEXT H
2920 F(I) = (RADINT / 3) * (T(1) + 4 * SUMEVE + 2 * SUMODD + T(N + 1))
2930 NEXT I
2940 SUMEVE = 0
2950 FOR H = 2 TO N STEP 2
2960 SUMEVE = SUMEVE + F(H)
2970 NEXT H
2980 SUMODD = 0
2990 FOR H = 3 TO N - 1 STEP 2
3000 SUMODD = SUMODD + F(H)
3010 NEXT H
3020 '
3030 '*************************************************************************
3040 'CALCULATE TYPE III SHEAR AND EFFECTIVE SHEAR AT EACH DATA POINT
3050 TIHV(NO) = ((LAMINT / 3) * (F(1) + 4 * SUMEVE + 2 * SUMODD + F(N + 1))) / AREA
3060 TIEFF(NO) = (1 / AREA) * (HOR(NO) - (2 * C ^ 2 * HS) / (5.5 * SIN(THETA / 2)) -
        (C ^ 2 * HS) / (TAN(THETA / 2)) - HFILM * (BMIN + C) * T)
3070 'UNITS FOR BOTH TIHV AND TIEFF ARE (N/m^2)
3080 TIHV(NO) = TIHV(NO) * .000001 'CONVERTS TIHV (N/m^2) TO (MPa)
3090 TIEFF(NO) = TIEFF(NO) * .000001 'CONVERTS TIEFF (N/m^2) TO (MPa)
3100 NEXT NO
3110 PRINT "HFILM = ", HFILM
3120 '
3130 '*************************************************************************
3140 'PRINT SHEAR DATA
3150 'TACT IS THE TOTAL INTERFACIAL SHEAR STRENGTH BASED ON THE HORIZONTAL AND
3160 'VERTICAL FORCES
```

```
3170 FOR NO = 1 TO SCANS
3180 FOR CH = 1 TO 3'CHANGE 1 BACK TO 0 FOR DISTANCE COLUMN
3190  'IF CH = 0 THEN SHEAR(NO,CH)=CM(NO) REMOVED TO INCREASE MEMORY
3200 IF CH = 1 THEN SHEAR(NO, CH) = TIHV(NO)
3210 IF CH = 2 THEN SHEAR(NO, CH) = 'TIEFF(NO)
3220 IF CH = 3 THEN SHEAR(NO, CH) = TIEFF(NO) + TIHV(NO)   'BOTH TIEFF AND TIHV
3230  'ACT OVER THE SAME AREA; AREAS CANCEL OUT IN FORCE BALANCE EQUATION.
3240 NEXT CH
3250 NEXT NO
3260 PRINT " "
3270 PRINT "   TIHV (MPa)  TIEFF (MPa)  TACT (MPa)"
3280 FOR NO = 1 TO SCANS
3290 FOR CH = 1 TO 3'CHANGE 1 BACK TO 0 FOR DISTANCE COLUMN
3300 PRINT USING "#######.####"; SHEAR(NO, CH); 'NOTE THE SUM IS THE ACTUAL
3310 PRINT CHR$(32);    '              SHEAR STRESS, TACT
3320 NEXT CH
3330 PRINT " "
3340 NEXT NO
3350 PRINT " "
3360 BEEP
3370  '
3380      '*************************************************************************
3390  'GENERATE SHEAR DATA FILE
3400 INPUT "DO YOU WISH TO SAVE THE SHEAR DATA  (Y/N)  ", QUES$
3410 IF QUES$ = "N" OR QUES$ = "n" GOTO 3550
3420 INPUT "ENTER NAME OF DATA FILE TO BUILD (IE SHEAR##.DAT)  ", FINAL$
3430 OPEN FINAL$ FOR OUTPUT AS 1
3440 FOR NO = 1 TO SCANS
3450 FOR CH = 1 TO 3 'CHANGE 1 BACK TO 0 FOR DISTANCE COLUMN
3460 PRINT #1, USING "#######.####"; SHEAR(NO, CH);
3470 PRINT #1, CHR$(9);
3480 NEXT CH
3490 PRINT #1, " "
3500 NEXT NO
```

```
3510 CLOSE #1
3520 PRINT " "
3530  '
3540      '*************************************************************************
3550 INPUT "WOULD YOU LIKE TO TRY ANOTHER EVALUATION  (Y/N)  ", QUES2$
3560 IF QUES2$ = "Y" OR QUES2$ = "y" GOTO 2000
3570 END
*****************************************************************************************
```

APPENDIX F - BESSEL FUNCTION EXPANSION

A modified Bessel function of the second kind to the n^{th} order and its derivative are expanded as follows [Ref. 27]:

$$k_n(x) \approx \sqrt{\frac{\pi}{2x}}\, e^{-x}\left[1+\frac{(\mu-1)}{8x}+\frac{(\mu-1)(\mu-9)}{2!(8x)^2}+\ldots\right] \qquad \textbf{(F.1)}$$

$$k'_n(x) \approx -\sqrt{\frac{\pi}{2x}}\, e^{-x}\left[1+\frac{(\mu+3)}{8x}+\frac{(\mu-1)(\mu+15)}{2!(8x)^2}+\ldots\right] \qquad \textbf{(F.2)}$$

where x is the argument of the function and much greater than n, and

$$\mu = 4n^2 \qquad \textbf{(F.3)}$$

n=1 for the first order, hence μ=4. For the application of this thesis, z is the argument and is defined as:

$$z = \frac{b\phi}{t} \qquad \textbf{(F.4)}$$

where

$$\phi = \sqrt{\frac{6(1-\nu)}{(4+\nu)}} \qquad \textbf{(F.5)}$$

ν is Poisson's ratio for the film.

LIST OF REFERENCES

1. Matthewson, M.J., "Adhesion Measurements of Thin Films by Indentation," *Applied Physics Letters*, v. 49, no. 21, pp. 1426-1428, 24 November 1986.

2. Ritter, J.E., Lardner, T.J., Rosenfeld, L., and Lin, M.R., "Measurement of Adhesion of Thin Polymer Coatings by Indentation," *Journal of Applied Physics*, v. 66, no. 8, pp. 3626-3634, 15 October 1989.

3. Matthewson, M.J., "Axi-Symmetric Contact on Thin Compliant Coatings," *Journal of the Mechanics and Physics of Solids*, v. 29, no. 2, pp. 89-113, 1981.

4. Valli, J., "A Review of Adhesion Test Methods for Thin Hard Coatings," *Journal of Vacuum Science and Technology*, v. A4, no. 6, pp. 3007-3014, November/December 1986.

5. Benjamin, P. and Weaver, C., "Adhesion of Metal Films to Glass," *Proceedings of the Royal Society of London*, v. A254, pp. 177-183, 1960.

6. Weaver, C., "Adhesion of Thin Films," *Journal of Vacuum Science Technology*, v. 12, no. 1, pp. 18-25, 1977.

7. Ritter, J.E., Rosenfeld, L., Lin, M.R., and Lardner, T.J., "Interfacial Shear Strength of Thin Polymeric Coatings on Glass," *Proceedings of the Materials Research Society Symposium*, v. 130, pp. 237-242, 1989.

8. Campbell, D.S., *Mechanical Properties of Thin Films*. Edited by L.I. Maissel and R. Glang, *Handbook of Thin Film Technology*, pp. 12-12 - 12-19, McGraw-Hill Book Company, 1970.

9. Lin, M.R., Ritter, J.E., Rosenfeld, L., and Lardner, T.J, "Measuring the Interfacial Shear Strength of Thin Polymer Coatings on Glass," *Journal of Materials Research*, v. 5, no. 5, pp.1110-1117, May 1990.

10. Fabes, B.D., Oliver, W.C., McKee, R.A., and Walker, F.J., "The Determination of Film Hardness from the Composite Response of Film and Substrate to Nanometer Scale Indentation," *Journal of Materials Research*, v. 7, no. 11, pp. 3056-3064, November 1992.

11. Valli, J., Mäkelä, U., Matthews, A., and Murama, V., "TiN Coating Adhesion Studies Using the Scratch Test Method," *Journal of Vacuum Science and Technology*, v. A3, no. 6, pp. 2411-2414, November/December 1985.

12. Julia-Schmutz, C. and Hintermann, H.E., "Microscratch Testing to Characterize the Adhesion of Thin Layers," *Surface and Coatings Technology*, v.48, pp. 1-6, 1991.

13. Benjamin, P. and Weaver, C., "Measurement of Adhesion of Thin Films," *Proceedings of the Royal Society of London*, v. A254, pp. 163-176, 1960.

14. Butler, D.W., Stoddart, C.T.H., and Stuart, P.R., "The Stylus or Scratch Method for Thin Film Adhesion Measurements: Some Observations and Comments," Journal of Physics D: Applied Physics, v.3, pp. 877-833, 1970.

15. Lascurain, D.P., *A Scratch Test for Measurement of Adhesion at Thin Film-Ceramic Interfaces*, Master's Thesis, Naval Postgraduate School, Monterey, California, March 1993.

16. Maan, N. and Van Groenou, A.B., "Low Speed Scratch Experiments on Steel," *Wear*, v. 42, pp. 365-390, 1977.

17. Valli, J. and Mäkelä, U., "Applications of the Scratch Test Methods for Coating Adhesion Assessment," *Wear*, v. 115, pp. 215-221, 1987.

18. Sekler, J., Steinman, P.A., and Hintermann, H.E., "The Scratch Test: Different Critical Load Determination Techniques," *Surface and Coatings Technology*, v. 36, pp. 519-529, 1988.

19. Hedenqvist, P., Olsson, M., and Jacobson, S., "Failure Mode Analysis of TiN-Coated High Speed Steel: *in situ* Scratch Adhesion Testing in the Scanning Electron Microscope," *Surface and Coatings Technology*, v. 41, pp. 31-49, 1990.

20. Bull, S.J., "Failure Modes in Scratch Adhesion Testing," *Surface and Coatings Technology*, v. 50, pp. 25-32, 1991.

21. Benjamin, P. and Weaver, C., "The Adhesion of Metals to Crystal Faces," *Proceedings of the Royal Society of London*, v. A274, pp. 267-273, 1963.

22. Bowden, F.P and Tabor, D., *The Friction and Lubrication of Solids*, Part I, pp. 10-22, Oxford University Press, 1950.

23. Thomas, G.B., Jr., *Calculus and Analytic Geometry*, p. 368, Addison-Wesley Publishing Company, 1968.

24. Interview between Y.W. Kwon, Associate Professor, Naval Postgraduate School, Monterey, California, and the author, 16 November 1993.

25. James, M.L., Smith, G.M., and Wolford, J.C., *Applied Numerical Methods for Digital Computation*, pp. 400-403, Harper Collins College Publishers, 1993.

26. Interview between R.A. Smith, Professor, United States Naval Academy, Annapolis, Maryland, and the author, 20 January 1994.

27. Bickley, W.G., comp., *Bessel Functions and Formulae*, University Press Cambridge, 1966.

INITIAL DISTRIBUTION LIST

	No. Copies
1. Defense Technical Information Center Cameron Station Alexandria, VA 22304-6145	2
2. Library, Code 52 Naval Postgraduate School Monterey, CA 93943-5002	2
3. Department Chairman, Code ME/Kk Department of Mechanical Engineering Naval Postgraduate School Monterey, CA 93943-5000	1
4. Professor I. Dutta, Code ME/Du Department of Mechanical Engineering Naval Postgraduate School Monterey, CA 93943-5000	2
5. LCDR E. Daniel Secor 703 Sonne Drive Annapolis, MD 21401	4
6. LT D.P. Lascurain 2709 Amherst Road Rocky Mount, NC 27804	1
7. Curricular Officer, Code 34 Department of Naval Engineering Naval Postgraduate School Monterey, CA 93942-5000	1
8. Mr. Kevin Beasley Building 2044 NSWC - Crane Division Crane, IN 47522	1
9. Mr. Pat Sullivan NCCOSC-RDT&E Division Code 551 271 Catalina Boulevard San Diego, CA 92110	1